

# Discerning Secluded Sector gauge structures

---

**Lisa Carloni, Johan Rathsmann and Torbjörn Sjöstrand**

*Theoretical High Energy Physics*

*Department of Astronomy and Theoretical Physics, Lund University,  
Sölvegatan 14A, SE 223-62 Lund, Sweden*

*E-mail:*

`lisa.carloni@thep.lu.se, johan.rathsmann@thep.lu.se, torbjorn@thep.lu.se`

## ABSTRACT:

New fundamental particles, charged under new gauge groups and only weakly coupled to the standard sector, could exist at fairly low energy scales. In this article we study a selection of such models, where the secluded group either contains a softly broken  $U(1)$  or an unbroken  $SU(N)$ . In the Abelian case new  $\gamma_v$  gauge bosons can be radiated off and decay back into visible particles. In the non-Abelian case there will not only be a cascade in the hidden sector, but also hadronization into new  $\pi_v$  and  $\rho_v$  mesons that can decay back. This framework is developed to be applicable both for  $e^+e^-$  and  $pp$  collisions, but for these first studies we concentrate on the former process type. For each Abelian and non-Abelian group we study three different scenarios for the communication between the standard sector and the secluded one. We illustrate how to distinguish the various characteristics of the models and especially study to what extent the underlying gauge structure can be determined experimentally.

**KEYWORDS:** Beyond Standard Model, Phenomenological Models.

---

## Contents

<b>1. Introduction</b>	<b>1</b>
<b>2. Overview of hidden sector scenarios</b>	<b>4</b>
2.1 Kinetic mixing scenarios	4
2.2 $Z'$ mediated scenarios	6
2.3 SM gauge boson mediated scenarios	6
2.4 Decays back to the SM	7
<b>3. Physics in the secluded sector</b>	<b>8</b>
3.1 Particles and their properties	8
3.2 Valley parton showers	10
3.2.1 Shower kinematics with massive hidden photons	11
3.2.2 Matrix element for radiation in production	15
3.2.3 Matrix element for radiation in decay	15
3.3 Hidden sector hadronization	16
3.4 Decays back into the SM sector	18
<b>4. Analysis of the different scenarios</b>	<b>19</b>
4.1 Basic distributions	20
4.2 $AM_{Z'}$ and $NAM_{Z'}$	24
4.3 $KMA_{\gamma_v}$ and $KMNA_{\gamma_v}$	26
4.4 SMA and SMNA	27
4.5 Angular distributions and event shapes	28
<b>5. Analysis: comparing <math>U(1)</math> and <math>SU(N)</math></b>	<b>31</b>
<b>6. Summary and Outlook</b>	<b>35</b>
<b>A. Scenario selection and setup</b>	<b>36</b>

---

## 1. Introduction

There are basically two ways in which one can envision new physics beyond the standard model that can be searched for at future colliders. One possibility is to have theories with new heavy particles coupling to the standard model with either the ordinary gauge couplings, as in supersymmetry, or with couplings of a similar magnitude. This implies heavy particle masses, in order to avoid collider constraints. The other possibility, which we want to explore in this paper, is that new light particles are ultra-weakly coupled to

the standard model particles, because they are not charged under the standard model gauge groups. Instead they couple to the ordinary matter through some heavy state which carries both SM charges and charges of a new unknown gauge group, also carried by the light states.

There have been several suggestions for theories with this type of secluded sectors (sometimes also called hidden valleys or dark sectors), proposing non-conventional new physics with unexpected and unexplored signals could show up at current colliders such as the Large Hadron Collider (LHC) or a future linear electron-positron collider.

One example is the so-called hidden valley scenarios by Strassler and collaborators [1, 2, 3, 4, 5, 6, 7], where the SM gauge group is extended by a new unspecified gauge group  $G$ . In the original paper [1] this group is a  $\mathcal{V}(1)' \times SU(N)$ . The new matter sector consists of  $v$ -particles (where  $v$  stands for “valley”), which are charged under the new gauge group and neutral under the standard one. The two sectors communicate via higher dimensional operators, induced either by heavy particle loops or by a  $Z'$  which can couple to both sectors.

An interesting feature of models with secluded sectors is that they naturally give rise to dark matter candidates. Likewise, some of the recently proposed dark matter models may present hidden sector features. Specific dark matter models developed in the last few years such as [8, 9, 10, 11, 12] suggest the existence of a GeV scale mass dark photon or scalar that is introduced to enhance the dark matter annihilation cross section, in order to fit the data from PAMELA [13, 14] and originally ATIC [15], although the latter data have later been superseded by more precise measurements from FERMI [16]. Here we will mainly be interested in models with dark photons originating from a softly broken  $\mathcal{V}(1)$ , which couple to standard model particles through so called kinetic mixing with the ordinary photon [17] through heavy particle loops in a similar way to the hidden valley scenarios.

The hidden valley-like theories and the dark matter models mentioned above share two features: the enlarging of the standard model symmetries to include a new gauge group  $G$  and the presence of new light particle sectors that are solely charged under this new gauge group. If the new light particles can decay into standard model particles, their existence could be inferred from their effect on standard model particle phenomenology. In [18] we studied the effects of the new gauge group radiation, specifically the kinematic effects of  $SU(3)'$  radiation from fermions charged under both the SM and the new gauge group on the kinematic distributions of visible particles. In this paper we address the issue of discerning between different gauge structures. Specifically, we want to outline the differences between signatures arising from a secluded sector broken  $\mathcal{V}(1)'$  gauge group with a light  $\gamma'$  and those arising from a confining  $SU(N)$ . In both cases we assume there is a mechanism for the secluded particles to decay back into the SM.

In order to distinguish which features of a given model are linked to the gauge group structure and which to the other details of the model, we consider different production processes and different mechanisms for the decay back into the SM. The various possibilities are summarized in Fig. 1. For the production we consider three mechanisms. In the first case the portal to the hidden sector is through kinetic mixing between the SM photon and a light  $\mathcal{V}(1)$  gauge boson. In the second case we have production via a  $Z'$ . In the kinetic

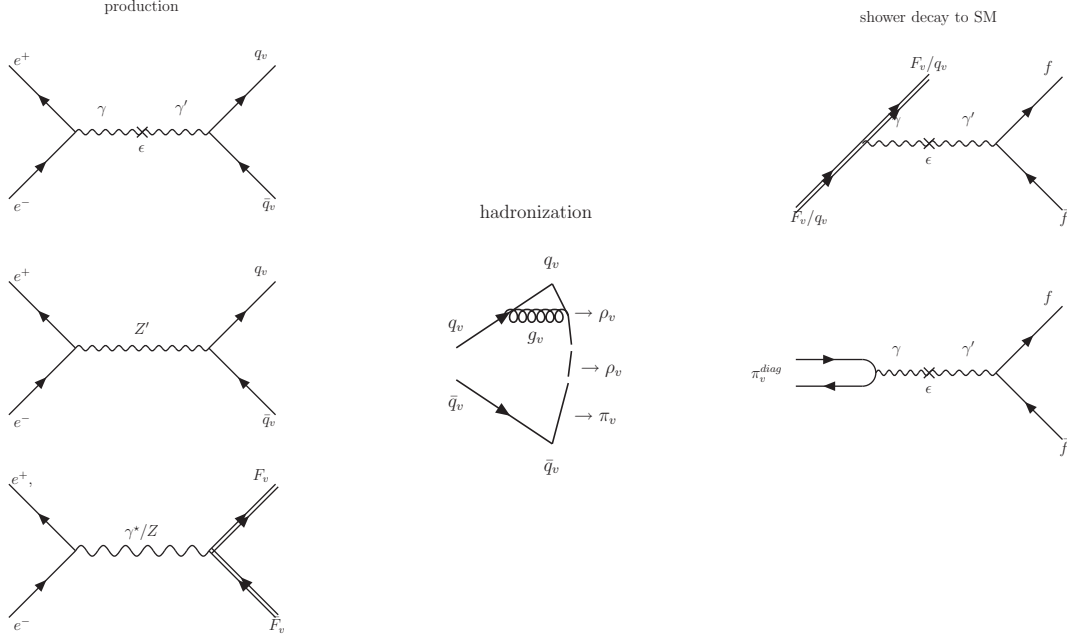


**Figure 1:** The different mechanisms for production, hadronization and decay that we consider as explained in the text.

mixing of  $\gamma$ - $\gamma_v$ , the  $\gamma_v$  is assumed to have a mass around 1-10 GeV and the mixing  $\epsilon$  is assumed to be  $\epsilon \sim 10^{-3}$ , while in the  $Z'$  case, the mass of the  $Z'$  would be around 1-6 TeV [1]. The third case is where the production happens via SM gauge bosons as in [18]. In this case the particles are assumed to have both SM charges and secluded sector ones. To distinguish them we will call them  $F_v$  in the following, to separate them from particles that are only charged under the secluded gauge group, which we call  $q_v$ . We will also assume that the  $F_v$  particles will decay into a standard model particle  $f$  and a secluded sector particle  $q_v$ , *i.e.*  $F_v \rightarrow f q_v$ .

If the particles of the secluded sector are charged under a non-Abelian  $SU(N)$  or a softly broken Abelian  $U(1)$  with a light  $\gamma_v$ , there will also be additional radiation of gauge bosons. In the former case, the  $v$ -gluons will be connected to the  $q_v$ s (produced directly or via the  $F_v$ s) and form a confined system which will then hadronize.

Depending on the nature of the secluded hadrons thus produced, they may then decay back into standard model particles through kinetic mixing or a heavy  $Z'$ . In both cases this decay can be very slow, so much so as to generate displaced vertices and other exotic signatures as for example discussed in [2]. In the case of  $\gamma_v$  radiation instead, the gauge bosons may decay directly back into the SM through kinetic mixing  $\gamma_v$ - $\gamma$ , while the  $q_v$ s will not be able to decay back into the SM since they carry the secluded gauge charge.

Thus, in both the non-Abelian and Abelian cases, we can have models where some of the particles produced will decay back into SM particles and some of them will be invisible. The questions we want to address is thus how the production of visible particles depends on the secluded gauge structure and whether it is possible to tell a non-Abelian and Abelian

gauge group apart also when other features of the models are very similar.

The paper is structured as follows. Section 2 gives a short overview of the general model considerations that underlie our studies, with particular emphasis on the production mechanisms that are relevant in various scenarios, and some comments on the decay mechanisms that lead to signals in visible distributions. In section 3 we provide a more in-depth overview of the new physics aspects that we have implemented in PYTHIA 8: the particle content, the parton showers, notably for the broken  $U(1)$  case, the hadronization in the secluded sector, and the decay back to the visible one. In Section 4 we proceed to describe the phenomenology of the various scenarios, in the context of an  $e^+e^-$  linear collider. While less interesting than a corresponding LHC phenomenology, it allows us to better highlight the relevant features of the model as such. In section 5 we further study distributions that could offer a discrimination between an Abelian and a non-Abelian scenario for the secluded sector. In Section 6 we summarize our findings, and give an outlook. Finally in Appendix 6 we provide information how the simulation of a wide range of scenarios can be set-up.

## 2. Overview of hidden sector scenarios

As already mentioned in the introduction there are many different types of models that can display hidden sectors and the common feature is that they communicate with the standard model through some heavy states. This communication can occur in many different ways and we will distinguish three different types in the following: via kinetic mixing, via a heavy  $Z'$ , and via heavy fermions that carry SM charges.

The common feature of the models we consider is that the SM group  $SU(3)_C \times SU(2)_L \times U(1)_Y$  is augmented by a new gauge group  $G$ . For each scenario we will consider two cases - one *Abelian* where  $G$  contains a softly broken  $U(1)$  with a light gauge boson  $\gamma_v$  and one *non-Abelian* where  $G$  contains an unbroken  $SU(N)$  factor mediated by a then massless  $g_v$ .

The particle content consists of  $q_v$  particles and/or  $F_v$  particles. With  $q_v$  particles we indicate fermions or scalars (with spin = 1/2, 0, 1) charged solely under the new gauge group. With  $F_v$  we indicate particles (spin  $s = 0, 1/2, 1$ ) which may couple to both secluded sector and standard model sector. Though in principle one could choose any spin assignment among the ones above, we have chosen to analyze the case in which  $F_v$  and  $q_v$  are fermions, except in the case when the  $q_v$ s are produced from a  $F_v$  decay when we assume them to be scalars. In addition, in all the scenarios we consider both  $F_v$  and  $q_v$  belong to the fundamental representation of the group  $G$ . Finally, the  $G$  sector charges are constrained by anomaly cancellation. For an example see [1].

### 2.1 Kinetic mixing scenarios

As already alluded to, one way of producing the secluded sector particles is through kinetic mixing. In the scenarios we wish to investigate, the SM  $U(1)$  (effectively the photon) mixes kinetically with a new GeV mass  $\gamma'$  and produces a pair of secluded sector particles, see Fig. 1. This mechanism is mostly relevant in the case when the secluded sector contains new fermions which are charged only under the new gauge group  $G$ . In addition we will

in this scenario only consider those cases when the SM particles are not charged under the new  $U(1)$ . Communication between the SM and secluded sectors then only comes from kinetic mixing between the standard model  $U(1)$  gauge boson and the new gauge boson, as described by

$$\mathcal{L}_{\text{kin}} = -\frac{1}{4}\epsilon_1 (F_1^{\mu\nu})^2 - \frac{1}{2}\epsilon F_1^{\mu\nu} F_{2,\mu\nu} - \frac{1}{4}\epsilon_2 (F_2^{\mu\nu})^2. \quad (2.1)$$

In the case of two  $U(1)$  gauge symmetries ( $U(1)_1 \times U(1)_2$ ), the non-vanishing mixing  $\epsilon$  arises naturally as one integrates out loops of heavy fermions coupling to both the associated gauge bosons [17] so long as there is a mass splitting among them. The relation between the size of the mixing and the mass splitting is given by

$$\epsilon = \frac{e_1 e_2}{16\pi^2} \ln \left( \frac{M_{12}^{(1)}}{M_{12}^{(2)}} \right), \quad (2.2)$$

where  $e_1$  and  $e_2$  are the gauge couplings of the fermions in the loop to the two  $U(1)$  gauge bosons,  $A_1$  and the new  $A_2$  respectively, and  $M_{12}^{(1)}$  and  $M_{12}^{(2)}$  are their masses. In general, the  $U(1)_1$  and the  $U(1)_2$  will not be orthogonal. One may however chose the  $U(1)_1$  generator so that the fermions that are only charged under  $U(1)_1$  do not have any charge shift, while those that couple to  $U(1)_2$  do [17].

For the case of non-Abelian groups,  $G_1 \times G_2 \times G_3$ , a mixing can come from the spontaneous breaking of the group down to  $H \times U(1)_1 \times U(1)_2$ . Also in this case the  $U(1)_1$  and the  $U(1)_2$  will not be orthogonal, as long as the three couplings associated to the unbroken symmetries are different.

The kinetic mixing mechanism has been used in model that want to describe various recent cosmic ray measurements in terms of dark matter models. The most important signal here is the positron excess observed by PAMELA [14]. At the same time, any model wanting to explain this excess also has to explain the absence of an anti-proton excess observed by PAMELA [13] and finally the measurements of the total electron and positron flux observed by the Fermi LAT collaboration [16]. The models are set up so that the dark matter particles will annihilate into a dark photon or scalar which couples to SM particles through kinetic mixing. The mass of the dark matter particle is then determined by the scale at which the positron excess is observed, to be of order 0.1–1 TeV.

In addition, the large positron excess observed also means that there must be some enhancement mechanism of the dark matter annihilation cross section. One way to do this is to invoke Sommerfeld enhancement<sup>1</sup> by introducing a light dark photon or scalar. The mass of the dark photon (or scalar) in these models is typically in the GeV range, which means that decays into  $\bar{p}$  and  $\pi^0$  are kinematically suppressed relative to the lepton decays and thus also explain the non-observation of any anti-proton excess by PAMELA[13].

A recent example of models that fits all these data is given by [19], but there are still large uncertainties due to cosmological assumptions such as the dark matter distribution and propagation of cosmic particles.

The dark gauge group  $G_{\text{dark}}$  is largely unspecified in these types of models except that it must contain a  $U(1)$  factor in order for the kinetic mixing with the SM photon. This

---

<sup>1</sup>Resummation of t-channel exchanges of a new light particle.

means that there could also be additional Abelian or non-Abelian factors in  $G_{\text{dark}}$ . In the following we will consider the cases when  $G_{\text{dark}}$  contains an additional  $U(1)$ , which is spontaneously broken giving a massive  $Z'$ , or an additional  $SU(N)$  factor giving a confining force for the secluded sector particles.

The phenomenology and constraints on these types of models at low energy  $e^+e^-$  colliders such as Belle, BaBar, DAΦNE, KLOE and CLEO have been studied by [20, 21, 22, 23].

## 2.2 $Z'$ mediated scenarios

The second type of scenarios we want to consider are those that are similar to the original hidden valley scenario [1] with a massive  $Z'$  coupling to both SM fermions and secluded sector ones. Thus, the processes we are interested in are when SM fermions annihilate into the secluded sector  $Z'$  which in turn gives a pair of secluded particles, as depicted in Fig. 1.

In these types of models it is typically assumed that the  $Z'$  acquires a mass by spontaneous symmetry breaking of a  $U(1)$  symmetry by a  $\langle\phi\rangle$  whereas the origin of the secluded sector  $\mathcal{V}(1)$  is not discussed.

The secluded sector particles that the  $Z'$  would decay to could be either charged solely under the valley gauge group  $G$  or charged under  $G$  and (parts of) the SM  $SU(3)_C \times SU(2)_L \times U(1)_Y$ . In the latter case, the particles would on the one hand have to be very massive (several hundreds of GeV) due to experimental constraints and on the other hand they would be more effectively produced through their SM couplings. Thus we will not consider this possibility more here. In contrast the particles charged solely under the secluded gauge group could be light with a mass in the 1 – 50 GeV range, thanks to the reduced coupling through the heavy  $Z'$ .

As a consequence of the heavy mass of the  $Z'$ , the  $s$ -channel pair production cross section will be peaked at  $\sqrt{s} \sim m_{Z'}$  and be suppressed at an  $e^+e^-$  collider unless  $\sqrt{s} \sim M_{Z'}$ . At a hadron collider the production of the  $Z'$  would be dominantly on-shell if the overall center of mass energy is large enough and there is enough support from the parton density functions.

In the original hidden valley model the secluded sector group also contains a confining  $SU(N)$ . Thus the produced secluded sector particles would have to hadronize into hadrons which are neutral under this  $SU(N)$ . Another possibility is that there is instead an additional  $\mathcal{V}(1)$  which would instead give radiation of  $\gamma$ 's.

Finally it should be noted that also in this case there is kinetic mixing between the  $Z$  and the  $Z'$ , which primarily is important for setting limits on the mass and couplings of the  $Z'$  from LEP as discussed in [1].

## 2.3 SM gauge boson mediated scenarios

The final type of scenario that we consider are ones where the "communicator" is charged under both the SM and new interactions. This scenario and its implementation into PYTHIA 8 has been described in [18] so here we only briefly recapitulate the main features.

In this model the new heavy communicator particle  $F_\nu$  would be pair produced with SM strength, which means that it would have to be quite heavy in order to not have been

already seen at colliders. Another consequence is that the communicator would decay into a SM and pure hidden sector particle, dubbed  $q_v$ , so that quantum numbers are conserved. In the simple case in which neither  $q_v$ s nor  $v$ -gauge bosons leak back into the SM, as in the scenario in [18], this entails a missing energy signal.

Also in this case, the secluded sector group can be either Abelian or non-Abelian. In both cases we will assume that the produced  $\gamma$ 's or hadrons can decay back to SM particles through kinetic mixing via loops of the  $F_v$  particles or via a  $Z'$ .

## 2.4 Decays back to the SM

First of all we mention again the case of secluded particles which are charged both under the SM and secluded gauge groups,  $F_v$ , which we assume decay according to  $F_v \rightarrow f q_v$ . All other particles produced by either of the mechanisms described above may decay back to SM particles as long as they do not carry any charge under the secluded gauge group. Essentially these decays will be through kinetic mixing with SM gauge bosons or through a heavy  $Z'$  as detailed below.

In the Abelian case, with a light secluded sector  $\gamma'$ , the  $q_v$ s will be stable, but the  $\gamma$ 's that are radiated in connection with the primary hard process will decay back to SM particles,  $\gamma' \rightarrow f \bar{f}$ . The strength of the kinetic mixing  $\epsilon$ , together with the available phase space, determines the decay width  $\Gamma_{\gamma' \rightarrow f \bar{f}}$ . Since the  $\gamma'$  is light, it will mainly mix with the standard model photon and thus the branching ratios for different channels will depend on the electric charge of the produced SM particles. In essence this means that the decays will be similar to a off-shell photon,  $\gamma^*$  with the virtuality given by  $m_{\gamma'}$ . We also note that if the kinetic mixing is small, the life-time could be so large as to give displaced vertices.

In the non-Abelian case the secluded sector hadrons may also decay back into the SM via kinetic mixing of the  $\gamma'$  with the SM photon or via a heavy  $Z'$ . In this case the phenomenology will depend on the number of light flavours  $N_{\text{flav}}$  in the secluded sector. In the following we will assume that  $N_{\text{flav}} \geq 2$  and only consider the case when the fundamental particles are fermions as in [1] although similar arguments can be made also in the case of scalar constituents. Thus, the bound states will be the secluded sector version of mesons, baryons and possibly also glueballs. For the decays back to SM particles, it is the meson states that are of primary interest and therefore we concentrate on them here.

With  $N_{\text{flav}}$  light flavours, there will be of the order  $N_{\text{flav}}^2$  mesons with a given spin out of which approximately  $N_{\text{flav}}$  are flavour neutral and can decay back into the SM via kinetic mixing or a  $Z'$ . The SM decay products will depend on the spin of the secluded meson. For a spin zero meson, helicity suppression leads to dominance by the heaviest SM particle available whereas for a spin 1 meson it will depend on the couplings to the particle mediating the decay, *i.e.* either to the photon in the case of kinetic mixing or to the  $Z'$ .

The phenomenology will thus depend on the relative production of spin-0 and spin-1 mesons and their masses. If the confinement scale  $\Lambda_v$  in the secluded sector is large compared to masses of the lightest secluded sector fermions the situation will be similar to QCD. In other words there will be a light spin-0  $\pi_v$  with mass much smaller than the spin-1  $\rho_v$ . Thus all  $\rho_v$  will decay to pairs of  $\pi_v$ s and the SM particles produced will be the heaviest one available.



If  $\Lambda_v$  is of the order of the masses of the lightest secluded sector fermions then the mass splitting between the spin-0 and spin-1 mesons will be small and thus the spin-1 meson will be metastable and instead decay back into the SM, again via either kinetic mixing or a  $Z'$ , but in this case, there not being any helicity suppression, the decay will be similar to that of an off-shell photon. Thus in this case there will also be an abundance of leptons produced along with hadrons.

If all constituent masses are much larger than the confinement scale, the lowest lying  $SU(N)$  neutral states would be glueballs as discussed in [7]. We do not discuss their phenomenology here. We will also not consider so called quirks [24] which are charged both under the SM  $SU(3)_C$  and a secluded  $SU(N)$  with the confinement scale  $\Lambda$  being much smaller than the  $F_v$  masses.

Finally we note that similarly to the Abelian case some of the secluded sector hadrons could be metastable and decay back into the detectors with displaced vertices.

### 3. Physics in the secluded sector

For the studies in this article we have developed a framework to simulate the physics of a secluded sector. It contains a flexible setup that can be used to study different production mechanisms, perturbative shower evolution scenarios, non-perturbative hadronization sequences and decays back into the visible sector. Parts of the framework were already in use for our previous study [18] but significant new capabilities have been added. These are available starting with PYTHIA 8.150. The physics content will be described in the following, while technical details on how to set up a variety of scenarios is outlined in Appendix A. The studies presented in this article only give a glimpse of the possibilities.

#### 3.1 Particles and their properties

The key aspect of a scenario is that of the valley gauge group  $G$ , which we allow to be either  $U(1)$  or  $SU(N)$ . The gauge bosons of these groups are named  $\gamma_v$  and  $g_v$ , respectively. The former can be broken or unbroken, i.e.  $\gamma_v$  can have a mass, while the latter is always unbroken so that  $g_v$  remains massless.

The rest of the particles, i.e. the “matter” content, fall into two main categories: those charged under both the SM and the  $v$  sector, and those that are pure  $v$ -sector particles.

For the doubly charged ones, dubbed  $F_v$ , 12 particles are introduced to mirror the Standard Model flavour structure, see Tab. 2 in the appendix. Each  $F_v$  particles couples flavour-diagonally to the corresponding SM particle. In addition to its SM charges, it is also put in the fundamental representation of  $G$ . For  $U(1)$  the charge is taken to be unity, while for  $SU(N)$  the “charge” is  $C_F = (N^2 - 1)/(2N)$  while pair production cross sections obtain a factor of  $N$  enhancement. Although the name suggests that the  $F_v$  are fermions, they can be spin 0, 1/2 or 1 particles. If the  $F_v$  particles have spin 1 then their production cross section depends also on the presence or not of an anomalous magnetic dipole moment.

The valley secluded sector further contains a purely  $G$  interacting sector. At the parton level this consists of  $q_v$ s, belonging to the fundamental representation of  $G$ . The name is introduced to reflect the similarities with the quark in QCD. The  $q_v$  particle is stable and

invisible to SM interactions. Its spin, 0 or 1/2, is adapted to the choice of spin made for  $F_v$ , in case the scenario allows for  $F_v \rightarrow f q_v$  decay, where  $f$  is a SM particle. The spin structure of the  $F_v \rightarrow f q_v$  decay is currently not specified, so the decay is isotropic.

In the  $G = U(1)$  scenarios only one  $q_v$  is assumed to exist.  $F_v$  decays, if allowed kinematically, are flavour diagonal,  $F_v^i \rightarrow f^i q_v$ , with a common (Yukawa) coupling strength. Given that both the  $F_v$ s and the  $q_v$ s have a unit of  $U(1)$  charge, they can radiate  $\gamma_v$  gauge bosons. If  $U(1)$  is unbroken the  $\gamma_v$  is massless and stable. For a broken symmetry,  $G = \mathcal{U}(1)$ , the  $\gamma_v$  can decay back to a SM fermion pair through the mechanisms discussed in the previous Section 2. For kinetic mixing or decay via a  $Z'$ , branching ratios by default are assumed to be proportional to the respective fermion coupling to the photon, whenever the production channel is allowed by kinematics. The  $\gamma_v$  decay can be either prompt or displaced.

If instead  $G = SU(N)$ , the massless  $g_v$  gauge bosons are self-interacting, such that the parton shower will also have to allow for  $g_v \rightarrow g_v g_v$  splittings, with no equivalence in the  $U(1)$  case. The self-interactions also lead to confinement, like in QCD. In Section 3.3 below we will explain how the resulting picture can be described in terms of “strings” stretched from a  $q_v$  end via a number of intermediate  $g_v$ s to a  $\bar{q}_v$  end. The string can break, by the production of new  $q_v \bar{q}_v$  pairs, to produce a set of  $v$ -mesons formed by the  $q_v$  of one break and the  $\bar{q}_v$  from an adjacent one. To first approximation these  $v$ -mesons would be stable, and so the whole  $v$ -hadronization process would be invisible. One would not even have the kind of indirect recoil effects that the  $v$ -shower can give. If kinetic mixing or decay via a  $Z'$  is assumed, it would again be possible to let the  $v$ -mesons decay back to a SM fermion pair.

With only one  $q_v$  species there would only be one kind of  $v$ -mesons, and so the choice would be between two extremes: either all the energy deposited in the hidden sector decays back to be visible, or none of it. The more interesting scenarios — e.g. in terms of offering a bigger challenge to sort out what is going on — are the ones where only part of the  $v$ -mesons can decay back. Therefore a variable number  $N_{\text{flav}}$  of separate  $q_v$  flavours are assumed to exist (at most 8 in the current implementation). This gives  $N_{\text{flav}}^2$  different possible  $v$ -meson flavour combinations, out of which only  $N_{\text{flav}}$  are flavour-diagonal and thus able to decay back into the SM sector. It would be possible to assign individual masses to the  $q_v$ s and  $v$ -mesons, but for now we assume one common  $q_v$  “constituent” mass and one common  $v$ -meson mass, twice as large as the former.

By analogy with QCD two separate spin states are assumed, denoted  $\pi_v$  and  $\rho_v$ . For now mass splitting is taken to be small, such that  $\rho_v \rightarrow \pi_v \pi_v$  is kinematically forbidden, as is the case in QCD for the  $s$  and heavier quarks. The decay of the flavour-diagonal mesons is different in the two cases: by helicity (non)conservation the  $\pi_v$  couplings to a pair of SM fermions  $f$  provides an extra factor  $m_f^2$ , an addition to the squared charge and phase space factors present for the  $\rho_v$  mesons.

In the confining  $SU(N)$  case also a  $v$ -glueball is introduced. It is only rarely used, to handle cases where the invariant mass of the invisible-sector fragmenting system is too large to produce one single on-shell  $v$ -meson and too small to give two of them. Then it is assumed that an excited  $v$ -meson state is produced, that can de-excite by the emission of

these invisible and stable  $g_v g_v$  bound states.

In summary, by default the  $v$ -particles with no SM couplings are not visible. Their presence can only be deduced by the observation of missing (transverse) momentum in the event as a whole. On top of this we allow two different mechanisms by which activity can leak back from the hidden sector. The first is the  $F_v \rightarrow f q_v$  decay and showers from the  $F_v$  and  $q_v$ , in the scenario in which  $F_v$  has both SM charges and  $G$  charges, as discussed in our previous article [18]. The second is the decay of SM gauge bosons produced through mixing by the  $G$  group gauge bosons in the kinetic mixing case, either the massive  $\gamma_v$  for  $U(1)$  or the diagonal  $v$ -mesons for  $SU(N)$ .

### 3.2 Valley parton showers

Parton showers (PS) offer a convenient approximation to higher-order matrix elements, which by the use of Sudakov form factors contain a resummation of virtual corrections to match the real emissions [26]. For the current studies, the PYTHIA  $p_\perp$ -ordered parton showers [27] are extended to the secluded sector, and the approach used to take into account massive radiating particles [28] must, for the  $U(1)$  scenario, be extended to the case where also the radiated gauge boson is massive. This section gives a summary of the showering framework, with emphasis on aspects new to this study (relative to [18]).

In the most general case, final-state QCD, QED and valley radiation are interleaved in one common sequence of decreasing emission  $p_\perp$  scales. That is, emissions of a SM  $g/\gamma$  or a hidden  $\gamma_v/g_v$  can alternate in the evolution of a  $F_v$ . Of course any of the related charges can be zero in a specific process, in which case the following expressions simplify accordingly. For the  $i$ 'th emission, the  $p_\perp$  evolution starts from the maximum scale given by the previous emission, with an overall starting scale  $p_{\perp 0}$  set by the scale of the hard process, or of the decay in which the radiating particle was produced. Thus the probability to pick a given  $p_\perp$  takes the form

$$\frac{d\mathcal{P}}{dp_\perp} = \left( \frac{d\mathcal{P}_{\text{QCD}}}{dp_\perp} + \frac{d\mathcal{P}_{\text{QED}}}{dp_\perp} + \frac{d\mathcal{P}_{\text{secl}}}{dp_\perp} \right) \exp \left( - \int_{p_\perp}^{p_{\perp i-1}} \left( \frac{d\mathcal{P}_{\text{QCD}}}{dp'_\perp} + \frac{d\mathcal{P}_{\text{QED}}}{dp'_\perp} + \frac{d\mathcal{P}_{\text{secl}}}{dp'_\perp} \right) dp'_\perp \right) \quad (3.1)$$

where the exponential corresponds to the Sudakov form factor. Implicitly one must also sum over all partons that can radiate.

To be more precise, radiation is based on a dipole picture, where it is a pair of partons that collectively radiates a new parton. The dipole assignment is worked out in the limit of infinitely many (hidden or ordinary) colours, so that only planar colour flows need be considered.

Technically the total radiation of the dipole is split into two ends, where one end acts as radiator and the other as recoiler. The recoiler ensures that total energy and momentum is conserved during the emission, with partons on the mass shell before and after the emission. Each radiation kind defines its set of dipoles. To take an example, consider  $q\bar{q} \rightarrow F_v \bar{F}_v$ , which proceeds via an intermediate  $s$ -channel gluon. Since this gluon carries no QED or hidden charge it follows that the  $F_v \bar{F}_v$  pair forms a dipole with respect to these two emission kinds. The gluon *does* carry QCD octet charge, however, so  $F_v \bar{F}_v$  do *not*

form a QCD dipole. Instead each of them is attached to another parton, either the beam remnant that carries the corresponding anticolour or some other parton emitted as part of the initial-state shower. This means that QCD radiation can change the invariant mass of the  $F_v \bar{F}_v$  system, while QED and hidden radiation could not. When a  $\gamma$  or  $\gamma_v$  is emitted the dipole assignments are not modified, since these bosons do not carry away any charge. A  $g$  or  $g_v$  would, and so a new dipole would be formed. For QCD the dipole between  $F_v$  and one beam remnant, say, would be split into one between the  $F_v$  and the  $g$ , and one further from the  $g$  to the remnant. For the secluded sector the  $F_v \bar{F}_v$  dipole would be split into two,  $F_v g_v$  and  $g_v \bar{F}_v$ . As the shower evolves, the three different kinds of dipoles will diverge further.

Note that, in the full event-generation machinery, the final-state radiation considered here is also interleaved in  $p_\perp$  with the initial-state showers and with multiple parton-parton interactions [29].

If the  $F_v$  fermion is allowed to decay into a SM and a hidden particle, one must also consider the hidden radiation from the hidden particle.

There is a clean separation between radiation in the production stage of the  $F_v \bar{F}_v$  pair and in their respective decay. Strictly speaking this would only be valid when the  $F_v$  width is small, but that is the case that interests us here.

In the decay  $F_v \rightarrow f q_v$  the QCD and QED charges go with the  $f$  and the valley one with  $q_v$ . For all three interactions the dipole is formed between the  $f$  and the  $q_v$ , so that radiation preserves the  $F_v$  system mass, but in each case only the relevant dipole end is allowed to radiate the kind of gauge bosons that goes with its charge. (Strictly speaking dipoles are stretched between the  $f$  or  $q_v$  and the “hole” left behind by the decaying  $F_v$ . The situation is closely analogous to  $t \rightarrow b W^+$  decays.)

The number of parameters of the hidden shower depends upon the scenario. In the case of the interleaved shower, there are only two, the most important one being one the coupling strength  $\alpha_v$ , i.e. the equivalent of  $\alpha_s$ . This coupling is taken to be a constant, i.e. no running is included.

From a practical point of view it is doubtful that such a running could be pinned down anyway, and from a theory point of view it means we do not have to specify the full flavour structure of the hidden sector. The second parameter is the lower cutoff scale for shower evolution, by default chosen the same as for the QCD shower,  $p_{\perp \min} = 0.4$  GeV.

### 3.2.1 Shower kinematics with massive hidden photons

Showers are expected to reproduce the soft and collinear behaviour of (leading-order) matrix elements (MEs), but there is no guarantee how trustworthy they are for hard wide-angle emissions. Therefore various correction techniques have been developed [26]. The technique we will use here is to generate trial emissions according to the PS, but then use the weights ratio ME/PS to accept emissions, i.e. PS times ME/PS equals ME. For this re-weighting recipe to work, obviously the ME weight has to be below the PS one, but the difference should not be too big or else the efficiency will suffer. It should also be noted that the ME/PS ratio is evaluated without including the Sudakov form factor of the shower, while the shower evolution itself does build up the Sudakov. By the veto algorithm it then

follows that the ME expression is exponentiated to provide the kernel of the Sudakov [30], a technique nowadays used as a key ingredient of the POWHEG approach [31]. The choice of shower evolution variable lives on in the integration range of the Sudakov, but for the rest the PS expressions disappear in the final answer.

In the past, this approach has only been developed for the emission of a massless gluon, however, and we now need to generalize that to an arbitrary combination of masses. A technical task is to recast the ME and PS expressions to use the same phase space variables, such that the ratio is well-defined.

We follow the existing approach of mapping the PS variables onto the ME ones. Below we therefore introduce the ME three-body phase space, subsequently how the PS variables populate this phase space, and finally how the presence of two shower histories can be taken into account.

Consider a dipole of invariant mass  $m_0$ , consisting of two endpoint partons 1 and 2, with nominal masses  $m_1$  and  $m_2$ . Assume that a shower emission occurs from the parton-1 dipole end, generating a new particle 3 with mass  $m_3$ . This implies that there was an intermediate off-shell state 13 with mass  $m_{13}$ . That is, the kinematics to describe is  $p_0 \rightarrow p_{13} + p_2 \rightarrow p_1 + p_3 + p_2$ . Averaging over the angular orientation of events, the MEs can be written in terms of the  $x_i = 2p_i p_0 / m_0^2$  and the  $r_i = m_i^2 / m_0^2$  variables, where the  $x_i$  reduce to energy fractions in the dipole rest frame, with normalization  $x_1 + x_2 + x_3 = 2$ . This means there are only two free independent variables, traditionally  $x_1$  and  $x_2$ .

The PS is instead described in terms of the  $p_{\perp\text{evol}}^2$  and  $z$  variables. In the soft and collinear emission limit these are well defined, but away from these limits different possibilities could be contemplated. Our choice is such that

$$m_{13}^2 = m_1^2 + \frac{p_{\perp\text{evol}}^2}{z(1-z)} , \quad (3.2)$$

or

$$p_{\perp\text{evol}}^2 = z(1-z)(m_{13}^2 - m_1^2) . \quad (3.3)$$

By standard two-body kinematics for  $p_0 \rightarrow p_{13} + p_2$  it follows that

$$x_2 = \frac{m_0^2 + m_2^2 - m_{13}^2}{m_0^2} = 1 + r_2 - r_{13} , \quad (3.4)$$

and thus  $x_1 + x_3 = 2 - x_2 = 1 + r_{13} - r_2$ . If  $m_1 = m_3 = 0$  one would further require that  $z = x_1 / (x_1 + x_3)$ . Taken together, this is enough to specify the three four-vectors  $p_2, p_1^{(0)}$  and  $p_3^{(0)}$ , up to three angles. These are chosen as follows: in the  $p_0$  rest frame parton 2 is assumed to keep its direction of motion when  $m_1 \rightarrow m_{13}$ , while 1 and 3 are selected to have an flat distribution in the azimuthal angle around the 13 direction, which is parallel with the 1 direction before the emission.

The kinematics for the case with massive partons 1 and 3 can then be constructed from the massless four-vectors as

$$p_1 = (1 - k_1)p_1^{(0)} + k_3 p_3^{(0)} \quad (3.5)$$

$$p_3 = (1 - k_3)p_3^{(0)} + k_1 p_1^{(0)} \quad (3.6)$$

$$k_{1,3} = \frac{m_{13}^2 - \lambda_{13} \pm (m_3^2 - m_1^2)}{2m_{13}^2} \quad (3.7)$$

$$\lambda_{13} = \sqrt{(m_{13}^2 - m_1^2 - m_3^2)^2 - 4m_1^2 m_3^2} \quad (3.8)$$

The physics content is that the directions of partons 1 and 3 in the  $p_{13}$  rest frame are retained, while their three-momenta are scaled down by a common factor sufficient to put the two partons on their mass shells. Since  $m_{13}$  is not changed by the operation it is necessary that  $m_{13} > m_1 + m_3$  for the rescaling to work.

The rescalings imply that

$$\frac{x_1}{x_1 + x_3} = \frac{x_1}{2 - x_2} = (1 - k_1)z + k_3(1 - z) = (1 - k_1 - k_3)z + k_3, \quad (3.9)$$

and thus

$$z = \frac{1}{1 - k_1 - k_3} \left( \frac{x_1}{2 - x_2} - k_3 \right). \quad (3.10)$$

Now we need to find the Jacobian to translate the shower emission rate from the  $(p_{\perp\text{evol}}^2, z)$  space to the  $(x_1, x_2)$  one. Note that  $m_{13}^2 = m_0^2(1 - x_2) + m_2^2$  is independent of  $x_1$ , and thus so are  $k_1$  and  $k_3$ . Therefore only the “diagonal” terms  $\partial p_{\perp\text{evol}}^2 / \partial x_2$  and  $\partial z / \partial x_1$  are needed.

The shower emission rate itself is

$$\frac{dp_{\perp\text{evol}}^2}{p_{\perp\text{evol}}^2} \frac{2 dz}{1 - z}. \quad (3.11)$$

Here an overall coupling factor  $C_F \alpha_v / 2\pi$  is omitted for simplicity. Also the Sudakov form factor is omitted, as already motivated. The  $z$ -dependent part may seem unfamiliar, but is an upper approximation to the more familiar  $q \rightarrow qg$  splitting kernel  $(1 + z^2)/(1 - z)$ , where the difference between the two is absorbed into the ME/PS weighting.

Put together, the shower emission rate translates into

$$\frac{dp_{\perp\text{evol}}^2}{p_{\perp\text{evol}}^2} = \frac{d(m_{13}^2 - m_1^2)}{m_{13}^2 - m_1^2} = \frac{dx_2}{1 - x_2 + r_2 - r_1}, \quad (3.12)$$

$$\begin{aligned} \frac{2 dz}{1 - z} &= \frac{2 dx_1}{(1 - k_1 - k_3)(2 - x_2)} \frac{1}{1 - \frac{1}{1 - k_1 - k_3} \left( \frac{x_1}{2 - x_2} - k_3 \right)} \\ &= \frac{2 dx_1}{x_3 - k_1(x_1 + x_3)}. \end{aligned} \quad (3.13)$$

When  $m_3 \rightarrow 0$ , and hence  $k_1 \rightarrow 0$ , this simplifies to the familiar expression [28]

$$W_{PS,1} = \frac{dp_{\perp\text{evol}}^2}{p_{\perp\text{evol}}^2} \frac{2 dz}{1 - z} = \frac{2 dx_1 dx_2}{(1 - x_2 + r_2 - r_1)x_3}. \quad (3.14)$$

If only parton 1 can radiate, as in  $F_v \rightarrow q_v + f \rightarrow q_v + \gamma_v + f$ , we are done. The fact that the MEs also contain a contribution from  $\gamma_v$  emission off the  $F_v$  does not change the picture, since that does not introduce any new singularities, and empirically the PS expression provides a valid upper limit.

For the radiation  $F_v \bar{F}_v \rightarrow F_v \bar{F}_v \gamma_v$  the sum of the two possible shower emissions are needed to match to the full MEs. Alternatively, and more conveniently, the ME expression can be split into two parts, each to be compared with only one shower history. This split is done in proportion to the respective propagator, i.e. assumed emission off parton  $i$  is proportional to  $1/(m_{i3}^2 - m_i^2)$ . The relative probability for parton 1 to radiate thus is

$$P_1 = \frac{m_{23}^2 - m_2^2}{(m_{13}^2 - m_1^2) + (m_{23}^2 - m_2^2)} = \frac{1 - x_1 + r_1 - r_2}{x_3} , \quad (3.15)$$

so that the ME weight to be associated with this dipole end is

$$W_{ME,1} = P_1 \frac{1}{\sigma_0} \frac{d\sigma}{dx_1 dx_2} dx_1 dx_2 . \quad (3.16)$$

Thus we arrive at the ME/PS correction factor

$$R_1 = \frac{W_{ME,1}}{W_{PS,1}} = \frac{(1 - x_1 + r_1 - r_2)(1 - x_2 + r_2 - r_1)}{2} \frac{1}{\sigma_0} \frac{d\sigma}{dx_1 dx_2} \times \frac{x_3 - k_1(x_1 + x_3)}{x_3} . \quad (3.17)$$

All the explicit dependence on  $m_3$  is located in  $k_1$  in the last term, but obviously implicitly the whole kinematics setup is affected by the value of  $m_3$ .

The matrix elements for the radiation off  $F_v \bar{F}_v$  are calculated with them as stable final-state particles. This means that, to preserve gauge invariance, they must be assigned the same mass. On the other hand, since they are supposed to decay, we allow them to have a Breit-Wigner mass distribution. To resolve this discrepancy, the real kinematics with two different masses is shifted to a fictitious one where  $F_v$  and  $\bar{F}_v$  have the same mass, and it is this fictitious one that is used in the three-parton matrix-element evaluation. As a guiding principle, the  $F_v$  and  $\bar{F}_v$  three-momenta are kept unchanged in the  $F_v \bar{F}_v$  rest frame, and only energy is shuffled so as to equalize the masses. Denoting the average mass  $\bar{m}$ , the conservation of three-momentum implies that

$$\sqrt{\frac{m_{12}^2}{4} - \bar{m}^2} = \sqrt{\frac{(m_{12}^2 - m_1^2 - m_2^2)^2 - 4m_1^2 m_2^2}{4m_{12}^2}} , \quad (3.18)$$

which gives

$$\bar{m}^2 = \frac{m_1^2 + m_2^2}{2} - \frac{(m_1^2 - m_2^2)^2}{4m_{12}^2} . \quad (3.19)$$

As above, the modified four-vectors  $\bar{p}_1$  and  $\bar{p}_2$  can be written as linear combinations of the original ones, with the constraints  $\bar{p}_1^2 = \bar{p}_2^2 = \bar{m}^2$  giving the solution

$$\bar{p}_1 = p_1 + \frac{m_2^2 - m_1^2}{2m_{12}^2} (p_1 + p_2) , \quad (3.20)$$

$$\bar{p}_2 = p_2 - \frac{m_2^2 - m_1^2}{2m_{12}^2} (p_1 + p_2) . \quad (3.21)$$

This translates into identical relationships for the modified matrix-element variables  $\bar{x}_1$  and  $\bar{x}_2$  in terms of the original  $x_1$  and  $x_2$  ones.

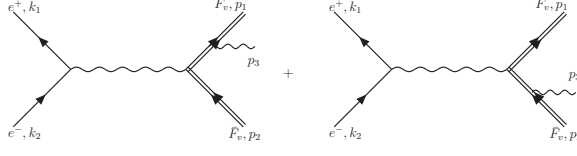


**Figure 2:** The Feynman diagrams for the production.

### 3.2.2 Matrix element for radiation in production

The implementation of the  $\mathcal{U}(1)$  has required the calculation of matrix element corrections  $|M|_{f\bar{f} \rightarrow F_v \bar{F}_v \gamma_v}^2$  for the pair production process  $f\bar{f} \rightarrow F_v \bar{F}_v \gamma_v$  described in Fig. 2. This has required the generalization of the matrix element corrections in [28] to the case of a massive photon:

$$\begin{aligned}
 |M|_{f\bar{f} \rightarrow F_v \bar{F}_v}^2 &= (1 - 4r_1)^{3/2}, \\
 \frac{|M|_{f\bar{f} \rightarrow F_v \bar{F}_v \gamma_v}^2}{|M|_{f\bar{f} \rightarrow F_v \bar{F}_v}^2} &= (r_3 + 2r_1)(-1 + 4r_1) \left( \frac{1}{(1 - x_1)^2} + \frac{1}{(1 - x_2)^2} \right) \\
 &\quad + \frac{-1 + 8r_1 - x_2}{1 - x_1} + \frac{-1 + 8r_1 - x_1}{1 - x_2} \\
 &\quad + \frac{2(1 - 6r_1 + 8r_1^2 + 4r_3r_1)}{(1 - x_1)(1 - x_2)} + 2.
 \end{aligned} \tag{3.22}$$

Here  $r_1 = r_2 = \bar{m}^2/m_0^2$  and  $r_3 = m_{\gamma_v}^2/m_0^2$ . (Expressions for  $r_1 \neq r_2$  have also been obtained but, by the preceding trick, are not needed.) Coupling constants have been omitted, as discussed before for the shower. Furthermore, to simplify calculations, the process is taken to proceed via the exchange of a scalar particle instead of a spin 1 gauge boson. The  $|M|_{f\bar{f} \rightarrow F_v \bar{F}_v \gamma_v}^2$  spin information, relevant for decay angular distributions, will be lost this way. Effects are known to be minor for the ME correction ratio [28]. As an illustration, the above expression reduces to  $(x_1^2 + x_2^2)/((1 - x_1)(1 - x_2)) + 2$  for  $r_1 = r_2 = r_3 = 0$ , where the first term is the familiar expression for  $e^+e^- \rightarrow \gamma^*/Z^* \rightarrow q\bar{q}$ , and the second finite term comes in addition for a spin 0 exchanged particle.

### 3.2.3 Matrix element for radiation in decay

The matrix elements corresponding to  $F_v \rightarrow q_v f \gamma_v$  are

$$\begin{aligned}
 |M|_{F_v \rightarrow q_v f}^2 &= (1 - r_1 + r_2 + 2q_2)\sqrt{(1 - r_1 - r_2)^2 - 4r_1r_2} \\
 \frac{|M|_{F_v \rightarrow q_v f \gamma_v}^2}{|M|_{F_v \rightarrow q_v f}^2} &= \frac{(r_3/2 + 2r_1^2 + r_2r_3/2 + q_2r_3 - 2r_1 - r_1r_3/2 - 2r_1r_2 - 4r_1q_2)}{(1 + r_2 - r_1 - x_2)^2} \\
 &\quad + \frac{(-2 + 2r_2^2 + 2r_1^2 + 2r_2r_3 - 4q_2 + 2q_2r_3 + 4q_2r_2 - 4r_1r_2 - 4r_1q_2)}{(1 + r_2 - r_1 - x_2)(r_3 - x_3)} \\
 &\quad + \frac{(-2 - r_3/2 - 2r_2 - 4q_2 + 2r_1)}{(1 + r_2 - r_1 - x_2)}
 \end{aligned} \tag{3.24}$$



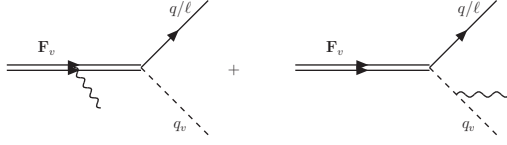


**Figure 3:** The Feynman diagrams for the  $F_v \rightarrow qv \ q/\ell$  decay.

$$\begin{aligned}
& + \frac{(-2 - r_3 - 2r_2 - r_2r_3 - 4q_2 - 2q_2r_3 + 2r_1 + r_1r_3)}{(r_3 - x_3)^2} \\
& + \frac{(-1 - r_3 - r_2 - 4q_2 + r_1 - x_2)}{(r_3 - x_3)} + 1 .
\end{aligned} \tag{3.25}$$

where  $r_1 = m_{q_v}^2/m_F^2$ ,  $r_2 = m_f^2/m_F^2$ ,  $r_3 = m_{\gamma_v}^2/m_F^2$  and  $q_2 = m_f/m_F = \sqrt{r_2}$ . The calculation has been done for the specific choice of  $F_v$  and  $f$  being fermions, and  $q_v$  a scalar, but again the result should be representative also for other spin choices.

### 3.3 Hidden sector hadronization

If the  $G$  group is the unbroken  $SU(N)$ , the gauge boson  $g_v$  is massless and the partons are confined. The picture therefore is closely similar to that of QCD, and we will use exactly the same framework to describe hadronization physics as in QCD: the Lund string model [32].

For the hidden sector, the model is most easily illustrated for the production of a back-to-back  $q_v \bar{q}_v$  pair, with the perturbative emission of additional  $g_v$ s neglected for now. In that case, as the partons move apart, the physical picture is that of a  $v$ -colour flux tube being stretched between the  $q_v$  and the  $\bar{q}_v$ . If the tube is assumed to be uniform along its length, this automatically leads to a confinement picture with a linearly rising potential,  $V(r) = \kappa r$ .

In order to obtain a Lorentz covariant and causal description of the energy flow due to this linear confinement, the most straightforward approach is to use the dynamics of the massless relativistic string with no transverse degrees of freedom. The mathematical, one-dimensional string can be thought of as parameterizing the position of the axis of a cylindrically symmetric flux tube.

Now consider the simple  $q_v \bar{q}_v$  two-parton event further. As the  $q_v$  and  $\bar{q}_v$  move apart from the creation vertex, the potential energy stored in the string increases, and the string may break by the production of a new  $q'_v \bar{q}'_v$  pair, so that the system splits into two colour singlet systems  $q_v \bar{q}'_v$  and  $q'_v \bar{q}_v$ . If the invariant mass of either of these systems is large enough, further breaks may occur, and so on until only  $v$ -mesons remain. A system with  $n$  primary  $v$ -mesons thus requires  $n - 1$  breaks  $q_{v,i} \bar{q}_{v,i}$  to produce a chain of  $v$ -mesons  $q_v \bar{q}_{v,1}$ ,  $q_{v,1} \bar{q}_{v,2}$ ,  $q_{v,2} \bar{q}_{v,3}$ ,  $\dots$ ,  $q_{v,n-1} \bar{q}_v$  stretching from the  $q_v$  end to the  $\bar{q}_v$  one.

The flavour of each  $q_{v,i}\bar{q}_{v,i}$  is supposed to be a random choice among the  $N_{\text{flav}}$  different flavours. Since all are taken to have the same mass, for now, they are also produced at the same rate. This thus also goes for the  $N_{\text{flav}}^2$  different  $v$ -meson flavour combinations. If the  $q_v$  are fermions then both pseudoscalar and vector  $v$ -mesons can be produced,  $\pi_v$  and  $\rho_v$ . Again disregarding possible effects of a mass splitting, simple spin counting predicts a relative production rate  $\pi_v : \rho_v = 1 : 3$ .

The possibility of higher excited states is disregarded, as is known to offer a good approximation for the QCD case. Also  $v$ -baryon production is left out, which is a 10% effect in QCD. For a generic  $SU(N)$  group a  $v$ -baryon needs to consist of  $N$   $v$ -quarks. This should lead to exceedingly tiny rates for  $N > 3$ , while  $N = 2$  could offer a more robust  $v$ -baryon production rate.

The space-time picture of the string motion can be mapped onto a corresponding energy-momentum picture by noting that the constant string tension implies that the  $v$ -quarks lose a constant amount of energy per distance traveled. The different breaks are space-like separated, but two adjacent breaks are constrained by the fact that the string piece created by them has to be on the mass shell for the  $v$ -meson being produced. The space-like separation implies that the fragmentation process can be traced in any order, e.g. from one of the endpoints inwards, while the constraint implies that there is only one kinematical degree of freedom for each new  $v$ -meson. Typically it is chosen to be  $z$ , the light-cone momentum fraction that the new  $v$ -meson takes from whatever is left in the system after previously produced  $v$ -meson have been subtracted off.

By symmetry arguments one arrives at the Lund-Bowler shape of the  $z$  probability distribution [33]

$$f(z) \propto \frac{1}{z^{1+bm_{q_v}^2}} (1-z)^a \exp\left(-\frac{bm_{m_v}^2}{z}\right), \quad (3.26)$$

where  $m_{m_v} \approx 2m_{q_v}$  is the mass of the produced  $v$ -meson. The equation contains two free parameters,  $a$  and  $b$ . Roughly speaking, these regulate the average rapidity spacing of the  $v$ -mesons, and the size of the fluctuations around this average. While  $a$  is dimensionless,  $b$  is not, which means that it becomes necessary to adjust  $b$  as  $m_{q_v}$  is changed. For instance, assume that the  $q_v$  mass is related to the strong-interaction scale  $\Lambda_v$ . Then, if  $\Lambda_v$ ,  $m_{q_v}$ ,  $m_{m_v}$  and the collision energy are scaled up by a common factor, we would want to retain the same rapidity distribution of produced  $v$ -mesons. This is achieved by rewriting  $bm_{m_v}^2 = (bm_{q_v}^2)(m_{m_v}^2/m_{q_v}^2) = b'(m_{m_v}^2/m_{q_v}^2)$ , where now  $b'$  can be assumed constant.

In addition to fluctuations in the longitudinal fragmentation, it is assumed that each new  $q'_v\bar{q}'_v$  pair produced when the string breaks also carries an opposite and compensating transverse momentum component. The  $p_\perp$  of the  $q_{v,i-1}\bar{q}_{v,i}$  meson is then given by the vector sum of its two constituent  $p_\perp$  values. The pair  $p_\perp$  naturally arises in a tunneling production process, which also leads to a Gaussian  $p_\perp$  distribution. The width  $\sigma$  of this Gaussian again should scale like  $\Lambda_v$ , so we rewrite as  $\sigma = (\sigma/m_{q_v})m_{q_v} = \sigma'm_{q_v}$ . When the  $v$ -mesons are allowed to acquire a  $p_\perp$  it should be noted that the  $m_{m_v}^2$  in eq. (3.26) must be replaced by  $m_{\perp m_v}^2 = m_{m_v}^2 + p_\perp^2$ .

In lack of further knowledge, it is convenient to assign  $b'$  and  $\sigma'$  values by analogy with standard QCD. To be more specific, we have in mind something like the  $s$  quark, with a

bare mass of the same order as  $\Lambda$ . For heavy quarks, like  $c$  and  $b$  in QCD, tunneling is suppressed, and the framework would have to be further modified. To assess uncertainties in a scenario, it would make sense to vary  $b'$  and  $\sigma'$  values over some range, say a factor of two in either direction.

So far, the emission of  $g_v$ s has been neglected. When it is included, more complicated string topologies can arise. Like in QCD, the complexity is reduced by using the planar or large- $N_C$  limit [34]. In it a  $v$ -gluon is assigned an incoherent sum of a ( $v$ -)colour charge and a different anticolour one. In a branching  $q_v \rightarrow q_v g_v$  the initial  $q_v$  colour is taken away by the  $g_v$  and a new colour-anticolour pair is stretched between the final  $q_v$  and  $g_v$ . Similarly  $g_v \rightarrow g_v g_v$  is associated with the creation of a new colour. That way partons nearby in the shower evolution also come to be colour-connected. This leads to a picture of a single string, consisting of several separate string pieces, stretching from one  $q_v$  end to the  $g_v$  it shares one colour with, on to the next colour-related  $g_v$ , and so on until the  $\bar{q}_v$  string end is reached. Several separate string pieces could have formed, had perturbative branchings  $g_v \rightarrow q_v \bar{q}_v$  been included, but, as in QCD,  $g_v \rightarrow q_v \bar{q}_v$  should be rare both in relation to the more singular  $g_v \rightarrow g_v g_v$  and in absolute terms.

The motion of a string with several gluon kinks can be quite complicated, but it is possible to extend the fragmentation framework of a single straight string also to the more complex topologies [35]. Basically the string will break up along its length by the production of new  $q'_v \bar{q}'_v$  pairs, with two adjacent breaks correlated in such a way that the  $v$ -meson produced between them is on the mass shell. Sometimes the two breaks will be on either side of a  $g_v$  string corner.

One of the key virtues of the string fragmentation approach is that it is collinear and infrared safe. That is, the emission of a gluon disturbs the overall string motion and fragmentation vanishingly little in the small-angle/energy limit. Therefore the choice of lower cut-off scale for parton showers is not crucial: letting the shower evolve to smaller and smaller scales just adds smaller and smaller wrinkles on the string, which still maintains the same overall shape.

The complete  $v$ -string fragmentation scenario contains a set of further technical details that are not described here. The key point, however, is that essentially all of the concepts of normal string fragmentation framework can be taken over unchanged. The one new aspect is what to do when the invariant mass of the hidden-valley system is too large to produce one single on-shell  $v$ -meson and too small to give two of them. As already explained, then the emission of  $v$ -glueballs is used to balance energy-momentum.

### 3.4 Decays back into the SM sector

Disregarding the trivial direct decay  $F_v \rightarrow f q_v$ , the main decay modes back into the SM are through  $\gamma_v$  kinetic mixing or  $Z'$  decay. For  $G = U(1)$  the  $\gamma_v$  therefore can decay to SM particles with the same branching ratios as a photon of corresponding mass, i.e.  $\propto e_f^2 N_c$ , with  $N_c = 1$  for leptons. For  $G = SU(N)$  only the flavour-diagonal mesons can decay, either with a  $\gamma_v$  or a  $Z'$ . (The former would imply that  $G = SU(N) \times U(1)$ , which would require some further extensions relative to the scenarios studied here.) A  $\rho_v$  meson, with spin 1, could have the same branching ratios as above, or slightly modified depending on

the  $Z'$  couplings. A  $\pi_v$  meson, with spin 0, would acquire an extra helicity factor  $m_f^2$  that would favor the heaviest fermions kinematically allowed. Should the  $\pi_v$  be scalar rather than pseudoscalar there would also be a further threshold suppression, in addition to the phase space one.

The decay back into the standard model would be accompanied by normal QED and QCD radiation, where relevant. Quarks and gluons would further hadronize, as described by the normal Lund string model. That model is not carefully set up to handle different exclusive states if the  $\gamma_v$  or  $\rho_v/\pi_v$  mass is very low, of the order 1 or 2 GeV, but should be good enough as a starting point. For studies that zoom in on one specific mass, more carefully constructed decay tables could be used instead.

#### 4. Analysis of the different scenarios

The tools described above allow us to simulate several different setups. We concentrate on the phenomenology of the six scenarios listed in Table 1. Three different production mechanisms are involved:  $s$ -channel pair production via kinetic mixing with the light  $\gamma_v$  ( $\text{KM}_{\gamma_v}$ ),  $s$ -channel pair production mediated by a  $Z'$  ( $\text{M}_{Z'}$ ) and  $s$ -channel pair production via SM gauge bosons (SM) and the  $F_v$  particles. For each of these production mechanisms an Abelian setup and a non-Abelian one are considered, labeled by A and NA respectively. Note that the Abelian/non-Abelian group we refer to in the following analyses correspond to the  $G$  gauge group, not to the production mechanisms. In the Abelian case  $G = \mathcal{U}(1)$ , while in the non-Abelian case  $G = SU(3)$ .

	production	radiation	hadronization	decay to SM
AM $_{Z'}$	$e^+e^- \rightarrow Z' \rightarrow q_v\bar{q}_v$	$q_v \rightarrow q_v\gamma_v$	—	$\gamma_v \rightarrow \text{SM}$
NAM $_{Z'}$	$e^+e^- \rightarrow Z' \rightarrow q_v\bar{q}_v$	$q_v \rightarrow q_v g_v, g_v \rightarrow g_v g_v$	$q_v\bar{q}_v \sim \pi_v/\rho_v$	$\pi_v/\rho_v \rightarrow \text{SM}$
KMA $_{\gamma_v}$	$e^+e^- \rightarrow \gamma_v \rightarrow q_v\bar{q}_v$	$q_v \rightarrow q_v\gamma_v$	—	$\gamma_v \rightarrow \text{SM}$
KMNA $_{\gamma_v}$	$e^+e^- \rightarrow \gamma_v \rightarrow q_v\bar{q}_v$	$q_v \rightarrow q_v g_v, g_v \rightarrow g_v g_v$	$q_v\bar{q}_v \sim \pi_v/\rho_v$	$\pi_v/\rho_v \rightarrow \text{SM}$
SMA	$e^+e^- \rightarrow \gamma^* \rightarrow E_v\bar{E}_v$	$q_v \rightarrow q_v\gamma_v$	—	$\gamma_v \rightarrow \text{SM}$
SMNA	$e^+e^- \rightarrow \gamma^* \rightarrow E_v\bar{E}_v$	$q_v \rightarrow q_v g_v, g_v \rightarrow g_v g_v$	$q_v\bar{q}_v \sim \pi_v/\rho_v$	$\pi_v/\rho_v \rightarrow \text{SM}$

**Table 1:** The six scenarios studied.

The phenomenology of the six scenarios is a function of the pair production cross section, which will in general depend upon the specific model realization of each setup. In particular, for the KM scenarios, the cross section will depend upon the size of the kinetic mixing parameter  $\epsilon$ , while for the  $Z'$  mediate ones on the mass of the  $Z'$  and on its couplings to the SM particles and to the  $v$ -quarks. The analysis is performed on per-event distributions, so as to factor out this model dependence. Assuming the same number of events are produced, the phenomenology of the setups will depend upon a different number of parameters. For the KMA $_{\gamma_v}$  and the AM $_{Z'}$  one must fix the  $q_v$  masses, the  $\gamma_v$  mass and the  $\mathcal{U}(1)$  coupling constant  $\alpha_v$ , while for the SMA production one must also fix the  $F_v$  masses. In the corresponding KMNA $_{\gamma_v}$ , AM $_{Z'}$  and SMNA one must fix the meson masses, but these will be connected to the  $q_v$  masses chosen, and furthermore the  $g_v$  remains

massless. We select a scenario in which  $m_{q_v} \sim \Lambda$ , so that  $m_{\pi_v} \sim m_{\rho_v}$ . This in turn ensures (as already described in section 2.4) that meson decay into SM lepton is not suppressed. For simplicity, in the following analysis we assume only one mass for all  $v$ -quark flavours, and only one common  $\pi_v/\rho_v$  mass  $m_{\pi_v/\rho_v} = 2m_{q_v}$ . One additional simplification in the following analysis, is that for the SM cases we assume the pair production of one single  $E_v$  belonging to the standard model doublet with no consideration for anomaly cancellation issues. In the non-Abelian case we have assumed simple proportions 1 : 3 for  $\pi_v : \rho_v$  production from fragmentation, which comes from spin counting when the  $q_v$  has spin 1/2. The branching ratios of the decays to standard model particles are fixed by the kinetic mixing mechanism.

We concentrate on the phenomenology of the six setups at an  $e^+e^-$  collider with center-of-mass (CM) energy of 800 GeV. A similar study for  $pp$  colliders like the LHC is also possible, and obviously more relevant in the near future, but makes it less transparent to compare and understand the properties of the models. Bremsstrahlung corrections have been included, and we shall see that these can give a non-negligible effect, whereas the machine-specific beamstrahlung has not. All of the figures in this section are based on a Monte Carlo statistics of 10000 events.

As a consequence of the  $e^+e^-$  collider choice, the events have a spherical symmetry rather than a cylindrical one, i.e. are described in terms of particle energy and  $(\theta, \phi)$  variables rather than in terms of  $E_T$  and  $(\eta, \phi)$ . The jet clustering algorithms are thus determined by the spherical topology and we primarily use the PYTHIA built-in **ClusterJet** Jade algorithm [36, 37]. The Jade algorithm is geared towards clustering objects nearby in mass, and so for clustering a variable number of fixed-mass  $\gamma_v/\pi_v/\rho_v$  systems it is more relevant than clustering e.g. in transverse momenta or angles.

#### 4.1 Basic distributions

The phenomenology of the six different setups is discussed in detail in dedicated subsections. We here would like to discuss the general features of the secluded sector signals and to introduce the observables we focus on.

One of the benefits of a Monte Carlo simulation is that one may look behind the scene, to study also the distributions of the invisible secluded sector particles. These can then be compared with the SM particle distributions to determine which features are governed by the secluded sector dynamics, and which come from the decays to the SM. In this spirit, Fig. 4 shows the number of  $\gamma_v$  gauge bosons emitted per event in the  $AM_{Z'}$  case. On the left we highlight the  $\alpha_v$  dependence, on the right the  $m_{\gamma_v}$  dependence. Not unexpectedly, the number of  $\gamma_v$  increases almost linearly with  $\alpha_v$ , up to saturation effects from energy-momentum conservation.

Compare this distribution with the corresponding non-Abelian  $AM_{Z'}$  case in Fig. 5 for the flavour diagonal  $\pi_v/\rho_v$ . Again the number of  $g_v$  grows with  $\alpha_v$ <sup>2</sup>, but the number of  $v$ -mesons does not primarily reflect this  $\alpha_v$  dependence. Instead the number of  $v$ -mesons

---

<sup>2</sup>Note that, in this case, the emission rate  $q_v \rightarrow q_v g_v$  is proportional to  $C_F \alpha_v$ , with  $C_F = (N^2 - 1)/(2N)$ , and  $g_v \rightarrow g_v g_v$  to  $N \alpha_v$ .

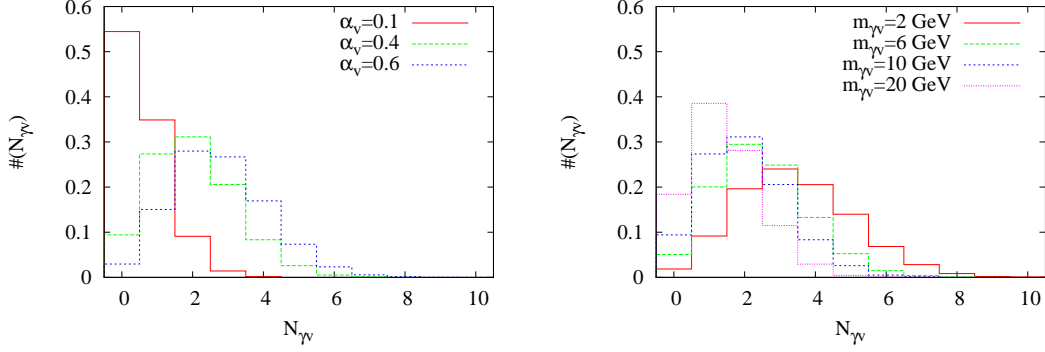


**Figure 4:**  $AM_{Z'}$ : the number of  $\gamma_v$  gauge bosons emitted per event. On the left we highlight the  $\alpha_v$  dependence, while on the right the  $m_{\gamma_v}$  dependence. On the left side  $m_{q_v} = 50$  GeV,  $m_{\gamma_v} = 10$  GeV and  $\alpha_v = 0.1, 0.4, 0.6$ , while on the right side  $m_{\gamma_v} = 2, 6, 10, 20$  GeV and the coupling is fixed at  $\alpha_v = 0.4$ .

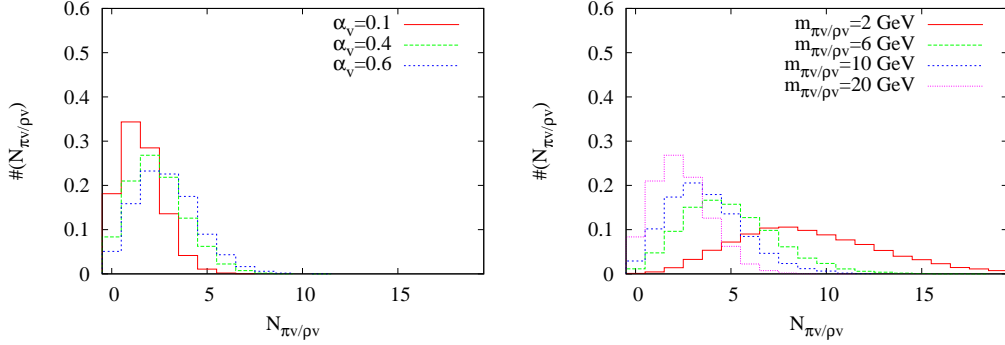


**Figure 5:**  $NAM_{Z'}$ : the number of flavour diagonal  $\pi_v/\rho_v$  mesons emitted per event. On the left we emphasize the  $\alpha_v$  dependence, while on the right the  $m_{\pi_v/\rho_v}$  dependence. On the left the meson mass is fixed at  $m_{\pi_v/\rho_v} = 10$  GeV and the coupling varies among  $\alpha_v = 0.1, 0.4, 0.6$ , while on the right side  $m_{\pi_v/\rho_v} = 2, 6, 10, 20$  GeV (which in turn implies  $m_{q_v} = 1, 3, 5, 10$  GeV), the coupling is fixed at  $\alpha_v = 0.4$  and the number of flavours is  $N_{\text{flav}} = 4$ .

produced by string fragmentation rather reflects the masses of the  $v$ -quarks (and thereby of the mesons) and the fragmentation parameters, see Fig. 5 right plot. Specifically, even with  $\alpha_v$  set to zero for the perturbative evolution, there would still be non-perturbative production of  $v$ -mesons from the single string piece stretched directly from the  $q_v$  to the  $\bar{q}_v$ . With  $\alpha_v$  nonzero the string is stretched via a number of intermediate  $g_v$  gluons that form transverse kinks along the string, and this gives a larger multiplicity during the hadronization.

Comparing the number of  $\gamma_v$  in Fig. 4 with the corresponding distributions in the other Abelian setups,  $KMA_{\gamma_v}$  and  $SMA$ , in Fig. 12 and Fig. 14 respectively, the two  $KMA_{\gamma_v}$  and  $AM_{Z'}$  setups produce similar distributions, while the  $SMA$  produces much fewer  $\gamma_v$ . The  $SMA$  difference is due to the more complicated kinematics, where the electrons from the  $E_v \rightarrow eq_v$  decays take away a large fraction of energy and momentum that then cannot be

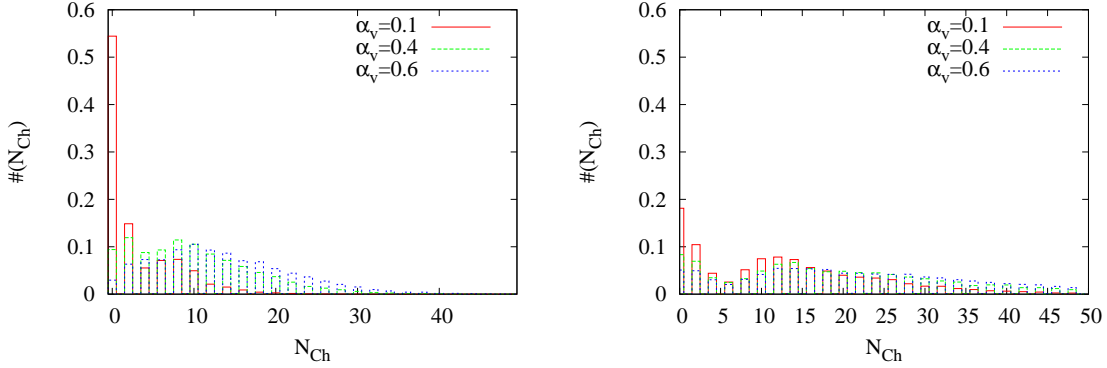


**Figure 6:**  $AM_{Z'}$ ,  $NAM_{Z'}$ :  $\alpha_v$  dependence of the overall number of charged particles emitted per event in the Abelian (left) and non-Abelian (right) case. For the Abelian cases  $m_{q_v} = 50$  GeV and  $m_{\gamma_v} = 10$  GeV, for the non-Abelian cases  $m_{q_v} = 5$ ,  $m_{\pi_v/\rho_v} = 10$  GeV.

used for  $\gamma_v$  emissions.

The average charged multiplicity of an event, Fig. 6, will be directly proportional to the number of  $\gamma_v/\pi_v/\rho_v$  produced. The trends from above are thus reproduced, that the non-Abelian multiplicity varies only mildly with  $\alpha_v$ , while the variation is more pronounced in the Abelian case. The constant of proportionality depends on the  $\gamma_v/\pi_v/\rho_v$  mass, with more massive states obviously producing more charged particles per state. This offsets the corresponding reduction in production rate of more massive  $\gamma_v/\pi_v/\rho_v$ , other conditions being the same. Similarly the number of jets should be proportional to the number of  $\gamma_v/\pi_v/\rho_v$  emitted, see further Sec. 4.2.

Without an understanding of the  $\gamma_v/\pi_v/\rho_v$  mass spectra, the mix of effects would make an  $\alpha_v$  determination nontrivial, especially in the non-Abelian case. Even with a mass fixed, e.g. by a peak in the lepton pair mass spectrum, other model parameters will enter the game. One such parameter is the number  $N_{\text{flav}}$  of  $q_v$  flavours. Since only  $1/N_{\text{flav}}$  of the  $\pi_v/\rho_v$  would decay back into the SM the visible energy is reduced accordingly. With all  $q_v$  having the same mass, the relation  $\langle E_{\text{visible}} \rangle / E_{\text{cm}} = 1/N_{\text{flav}}$  works fine to determine  $N_{\text{flav}}$ , but deviations should be expected for a more sophisticated mass spectrum. Furthermore the  $\pi_v : \rho_v$  mix, with different branching ratios for the two, needs to be considered. If the  $\pi_v$  fraction is large, the number of heavy leptons and hadrons produced may increase substantially, see [1].

In Fig. 7 we show the energy spectra of the hidden sector  $\gamma_v$  and  $\rho_v/\pi_v$ . Note the difference between the  $NAM_{Z'}$  setup and the  $KMNA\gamma_v$  one. This is due to the difference in the amount of initial-state radiation in the two cases, as discussed in Sec. 4.3 and shown in Fig. 11.

The energy and momenta of the  $v$ -sector particles not decaying back into the SM is the prime source of the missing  $p_{\perp}$  distributions,<sup>3</sup> see Fig. 8. In each of the six setups there is only one source of missing energy. In the Abelian ones it is the  $q_v$ s that escape

<sup>3</sup>with some extra effects from neutrinos e.g. in  $b$ ,  $c$  and  $\tau$  decays, included in the plots but here not considered on their own.

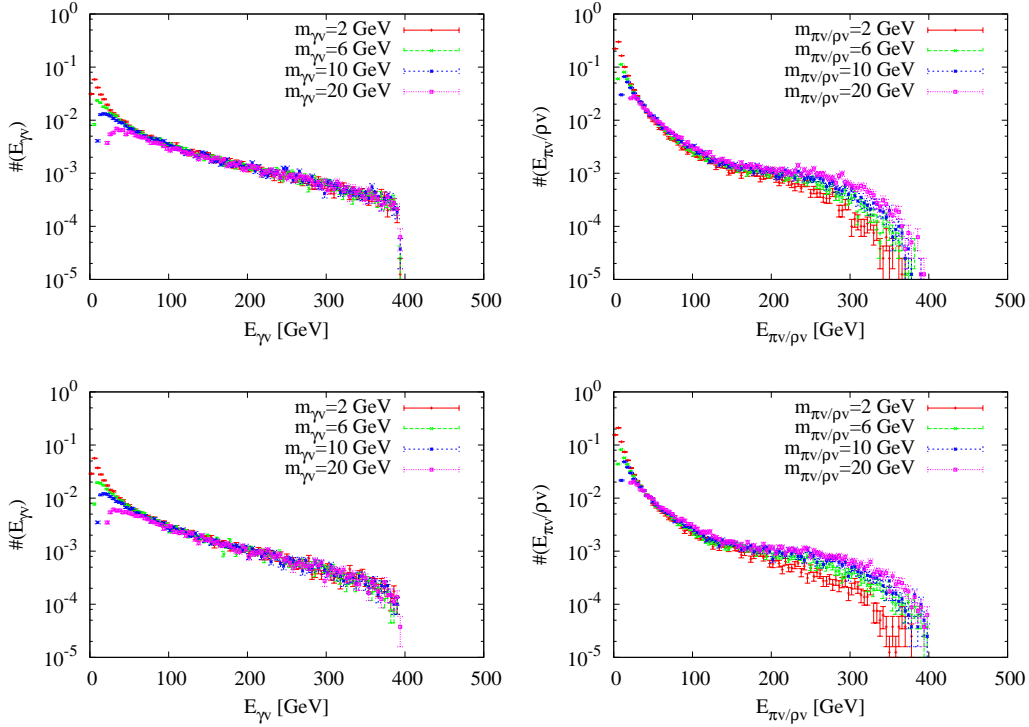


**Figure 7:**  $M_{Z'}$  vs  $KM_{\gamma_v}$ : the energy spectrum of the  $\gamma_v$  and diagonal  $\pi_v/\rho_v$  emitted per event. On top: left side shows the energy distribution for  $AM_{Z'}$ , the right side shows the corresponding one for  $NAM_{Z'}$ . Bottom: left side shows the energy distribution for  $KMA_{\gamma_v}$ , right side shows  $KMNA_{\gamma_v}$ . For the abelian cases  $m_{q_v} = 50$  GeV, for the non abelian cases  $m_{q_v} = m_{\gamma_v}/2$ . In all four cases  $\alpha_v = 0.4$ .

detection, while in the non-Abelian ones it is the stable non-diagonal  $v$ -mesons. For  $KMA_{\gamma_v}$  the falling Abelian  $\not{p}_\perp$  spectra are easily understood from the bremsstrahlung nature of the  $\gamma_v$  emissions. The spike at  $\not{p}_\perp = 0$  comes from events without any emissions at all, where all the energy is carried away by the invisible  $q_v$ s, and would hardly be selected by a detector trigger. (ISR photons might be used as a trigger in this case, but with irreducible backgrounds e.g. from  $Z^0 \rightarrow \nu\bar{\nu}$  it is not likely.). In the KMNA case the momentum of non-diagonal  $v$ -mesons does not leak back, this again allows a falling slope and a spike at  $\not{p}_\perp = 0$ , for events in which equal amount of energy in the non-diagonal mesons radiated from either side of the  $q_v\bar{q}_v$  system. For the SMA and SMNA scenarios, on the other hand, the starting point is the pT imbalance that comes from the  $e^+$  and  $e^-$  from the  $E_v$  and  $\bar{E}_v$  decays, which have no reason to balance each other. So even without  $\gamma_v$  emission, or diagonal  $\pi_v/\rho_v$ , there will be a  $p_\perp$  imbalance.

In the SMNA case, though the spectrum is shifted towards lower missing  $\not{p}_\perp = 0$  because on average a higher number of mesons are radiated, so it is less likely to have an event with the two leptons back-to-back. There could also be  $\not{p}_\perp = 0$  cases in which all the mesons are flavour diagonal and all the energy-momenta decays back into the SM, but these events are very rare.



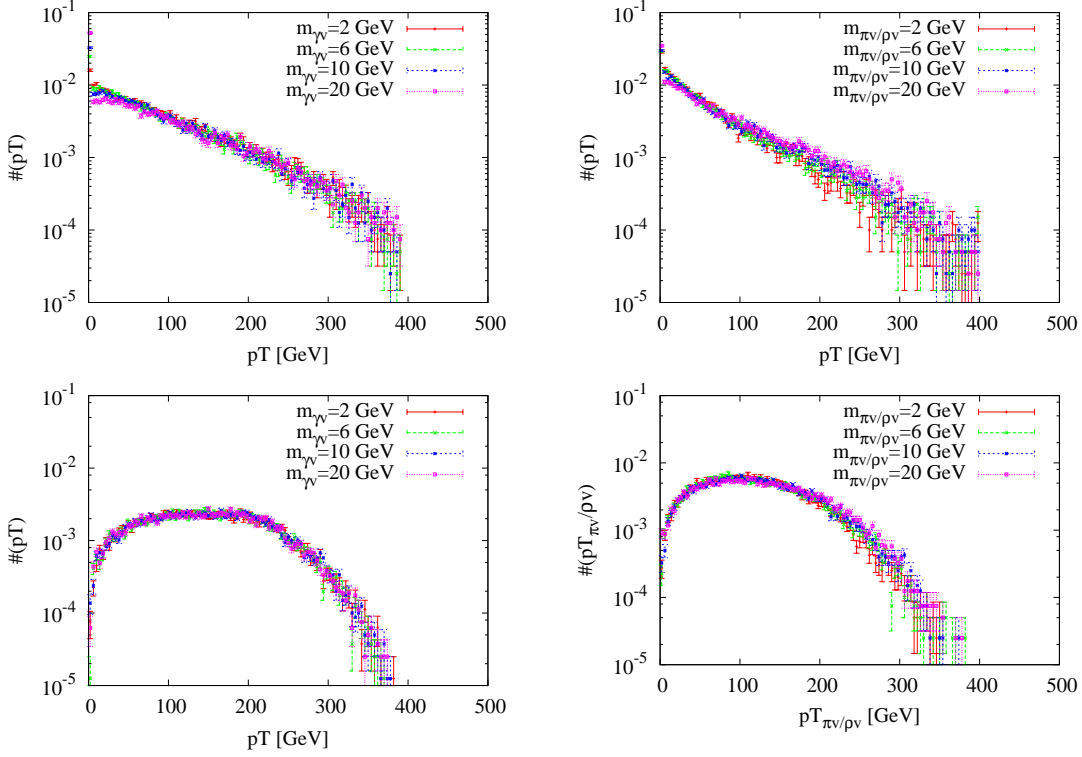


**Figure 8:**  $KMA_{\gamma_v}$ ,  $KMNA_{\gamma_v}$ ,  $SMA$ ,  $SMNA$ : the  $\not{p}_\perp$  spectrum in each event. For the Abelian cases (left) the  $\not{p}_\perp$  is due to the  $q_v$  escaping detection. For the non-Abelian cases (right) it is due to the  $v$ -flavoured mesons not decaying into SM particles. In the Abelian cases  $m_{q_v} = 50$  GeV, while in the non-Abelian cases (right)  $m_{q_v} = 1, 3, 5, 10$ . For all plots  $\alpha_v = 0.4$ .

In the Abelian case, the missing  $p_\perp$  distribution is directly connected to the mass parameter values  $m_{q_v}$  and, in the SMA case, to the  $m_{E_v}$ . The value of  $m_{q_v}$  in the KM/ $Z'$  mediated cases may be extracted from the kinematic limit given by the “shoulder” of the distribution. In the SM-mediated case, where two different fermion mass scales are involved, one can extract a relationship for the relative size of the two from lepton energy distributions such as the one in Fig. 16, see [18] for details. The distribution that directly pinpoints the mass of the particle decaying back into the SM, though, is the invariant mass of the lepton pairs produced, and that of the hadronic jets. We will discuss these distributions in the sections dedicated to each scenario.

## 4.2 $AM_{Z'}$ and $NAM_{Z'}$

In discussing the phenomenology of the different scenarios we will describe the  $v$ -sector particle distributions first, then the visible particle distributions followed by the jet distributions.

The number of particles of  $\gamma_v$  photons emitted in the  $AM_{Z'}$  and  $NAM_{Z'}$  scenarios was described in Fig. 4 and Fig. 5 in the previous section. The difference between the Abelian and non-Abelian dependence on the  $\alpha_v$  and  $m_{\gamma_v/\pi_v/\rho_v}$  parameters has already been highlighted in the same Sec. 4.1, as well as the  $\gamma_v/\pi_v/\rho_v$  energy distributions, the

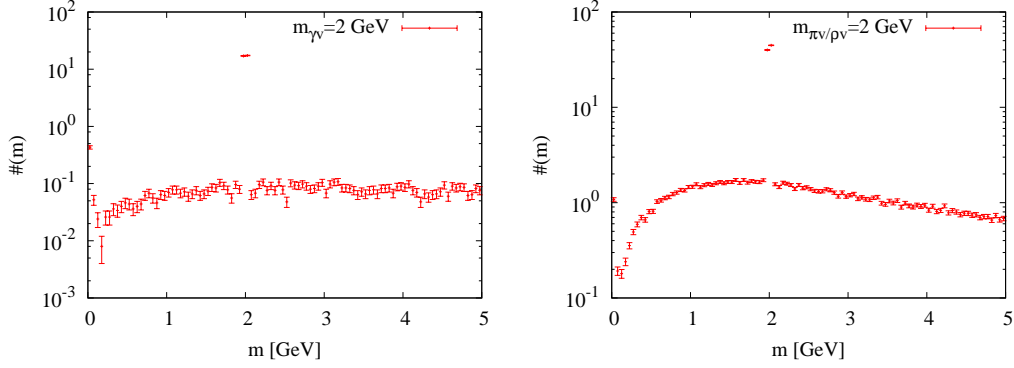


**Figure 9:**  $AM_{Z'}$  and  $NAM_{Z'}$ . The distribution of the invariant mass of the lepton pairs. Note the peak at 2 GeV, in both cases corresponding to the mass to be reconstructed  $m_{\gamma_v} = m_{\rho_v/\pi_v}$ . On the left, in the Abelian case,  $m_{q_v} = 50$  GeV, while on the right, in the non-Abelian case,  $m_{q_v} = 1$  GeV. The coupling is fixed at  $\alpha_v = 0.4$ .

charged multiplicity and the  $\not{p}_\perp$  spectrum. The difference between  $KMA_{\gamma_v}$  and SMA was also discussed.

The difference between the Abelian and non-Abelian  $\not{p}_\perp$  distribution in Fig. 8 is more subtle. In the Abelian case an event has maximum  $p_\perp$  imbalance when one of the  $q_v/\bar{q}_v$  produced emits a collinear  $\gamma_v$  which takes most of the  $q_v$  ( $\bar{q}_v$ ) momentum while the other  $v$ -quark has no emission and goes undetected. The more  $\gamma_v$  are emitted, the less likely it is that the undetected  $\bar{q}_v$  will have maximal energy. This remains true for all the  $m_{\gamma_v}$  contemplated (except in the low- $p_\perp$  region). In the non-Abelian case, to have large  $p_\perp$  imbalance the event must produce few energetic mesons back-to-back and have the mostly flavoured mesons at one end and mostly flavour neutral mesons at the other end. When the meson mass is lower, there is a higher probability of the string producing a large number of mesons and the likelihood of having large  $\not{p}_\perp$  falls rapidly. When the meson masses are higher and fewer  $\pi_v/\rho_v$  are produced the high  $\not{p}_\perp$  distribution falls off less rapidly.

The  $\gamma_v/\pi_v/\rho_v$  mass can be extracted from the lepton pair invariant mass, where it shows up as a well-defined spike, Fig. 9. (The additional spike near zero mass is mainly related to Dalitz decay  $\pi^0 \rightarrow e^+e^-\gamma$ .) Once the mass is known, the remaining hadrons and photons may be clustered using the Jade algorithm, with  $m_{\gamma_v/\pi_v/\rho_v}$  as the joining scale. The corresponding number of jets and invariant mass distribution for the hadronic jets is given in Fig. 10. The jet invariant mass distribution clearly shows the peaks connected to the invariant mass of the  $\gamma_v$ . The background comes from several sources. The spike at zero mass is mainly related to ISR photons; although we assume no detection within 50 mrad of the beam directions, some isolated photons do show up above this angle and form jets on their own. When kinematically possible,  $\tau$  decays and  $c$  and  $b$  decays will also occur. These contain neutrino products that reduce the visible mass, thus contributing to a continuum below the mass peak. Finally, misidentifications among partly overlapping systems leads to tails on both sides of the peak.

An efficient clustering algorithm should maintain the ratio between the average number of  $\gamma_v$  particles produced and the number of jets found, as is confirmed by comparing the

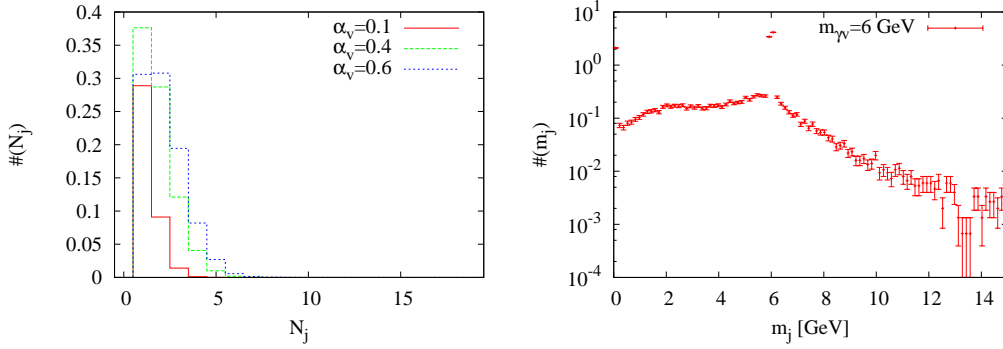


**Figure 10:**  $AM_{Z'}$ : the number of jets per event and the distribution of the invariant mass of the jets. In both plots the  $q_v$  mass is  $m_{q_v} = 50$  GeV. The left side shows the  $\alpha_v$  dependence for  $m_{\gamma_v} = 10$  GeV, while the right side shows the jet invariant mass distribution for  $\alpha_v = 0.4$  and  $m_{\gamma_v} = 6$  GeV. The jet reconstruction algorithm is Jade, with  $m_{\text{cut}}$  corresponding to the  $\gamma_v$  mass. Note the peak at 6 GeV.

plots on left side of Figs. 4 and 10. In this particular exercise we have relied on the extraction of the relevant mass scale from the lepton pair invariant mass distribution. This should be guaranteed by the presence of leptons in all six scenarios. Specifically, if the only way to decay back into the SM is via kinetic mixing, the  $\gamma_v \rightarrow SM$  branching ratios are fixed by the off-shell  $\gamma^*$  branching ratios. In the non-Abelian case the absence of a spin 1  $v$ -meson would reduce the rate of  $e^+e^-$  and  $\mu^+\mu^-$  pairs by helicity suppression. However, also in such scenarios, a simple trial-and-error approach with a range of jet clustering scales would suffice to reveal a convincing jet mass peak.

More information about the event and the model parameters can be extracted from the angular distributions in Sec. 4.5.

#### 4.3 $KMA_{\gamma_v}$ and $KMNA_{\gamma_v}$

The  $Z'$  mediated and  $\gamma_v$  mediated setups are effectively very similar, once the difference in coupling constants is factored out. The phenomenology can appear rather different, however, because of the initial state radiation from the electron/positron beams. To view this, recall that the photon bremsstrahlung spectrum is spiked at small energy fractions,  $\propto dz_\gamma/z_\gamma$ , and that therefore the electron-inside-electron PDF roughly goes like  $dz_e/(1-z_e)$ , with  $z_e = 1 - z_\gamma$ . In the case of a  $\gamma$  or light  $\gamma_v$  propagator, behaving like  $1/\hat{s} = 1/(z_e s)$ , this combines to give a  $dz_e/(z_e(1-z_e)) = dz_\gamma/((1-z_\gamma)z_\gamma)$  spectrum. The complete description includes the emission of multiple photons off both incoming beams, but the key features above described are readily visible in Fig. 11. Specifically, the spike at  $E_{\text{ISR}} = 400$  GeV corresponds to the emission of an energetic photon on one side only, while the non-negligible tail above that requires hard emissions on both sides.

Note that while the number of  $v$ -particles produced are similar for  $KMA_{\gamma_v}$  and  $AM_{Z'}$  in the Abelian case, Fig. 4 vs. Fig. 12, they are different in the non-Abelian case, Fig. 5 vs. Fig. 13. Specifically, the higher average multiplicity in the non-Abelian case leads to

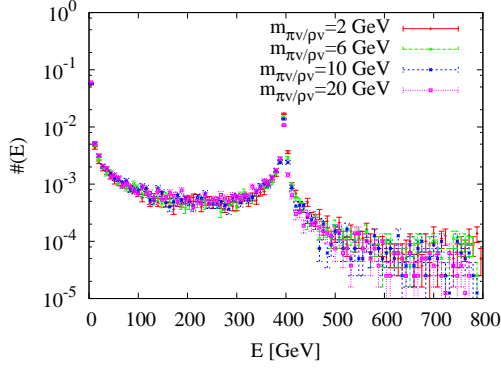


**Figure 11:**  $KMNA_{\gamma_v}$ : The total energy radiated in ISR photons. Note the spike around 400 GeV: a large fraction of the events will have a reduced  $\hat{s}$  due to IS photon emission. The  $q_v$  mass is fixed by  $m_{q_v} = m_{\pi/\rho_v}/2$ .

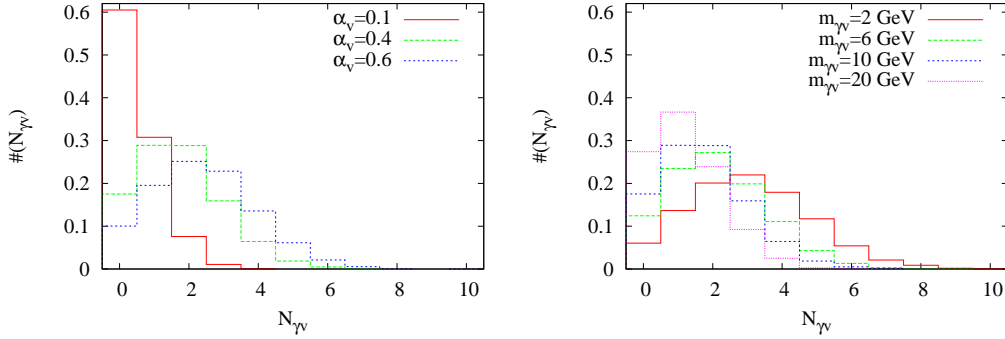


**Figure 12:**  $KMA_{\gamma_v}$ : the number of  $\gamma_v$  gauge bosons emitted per event. On the left we emphasize the  $\alpha_v$  dependence, while on the right the  $m_{\gamma_v}$  dependence. In both plots the  $q_v$  mass is  $m_{q_v} = 10$  GeV. On the left side  $m_{\gamma_v} = 10$  GeV and  $\alpha_v = 0.1, 0.4, 0.6$ , while on the right side  $m_{\gamma_v} = 2, 6, 10, 20$  GeV and the coupling is fixed at  $\alpha_v = 0.4$ .

a double spike in the distribution, a normal one from events with little ISR and an extra low-multiplicity one from events with much ISR.

#### 4.4 SMA and SMNA

The number of  $v$ -particles produced in the standard model mediated scenarios is shown in Fig. 14, and the energy of the  $\gamma_v$  photons and of the  $v$ -mesons in Fig. 15. The kinetic boundary  $E^{\max}$  is different in the two cases, owing to the choice of  $m_{q_v} = 50$  GeV in the Abelian case. This reduces the energy available for  $\gamma_v$  emissions. The  $\not{p}_\perp$  distribution was shown in Fig. 8 and has already been discussed.

The most important distribution to pinpoint the masses of the model is the lepton energy spectrum, Fig. 16. In this case leptons may come from both the kinetic mixing decays of the  $\gamma_v$  and from the decays of the  $E_v$  into  $eq_v$ . The energy spectra are very different in the two cases. The leptons coming from the  $E_v$  decays tend to be highly energetic,

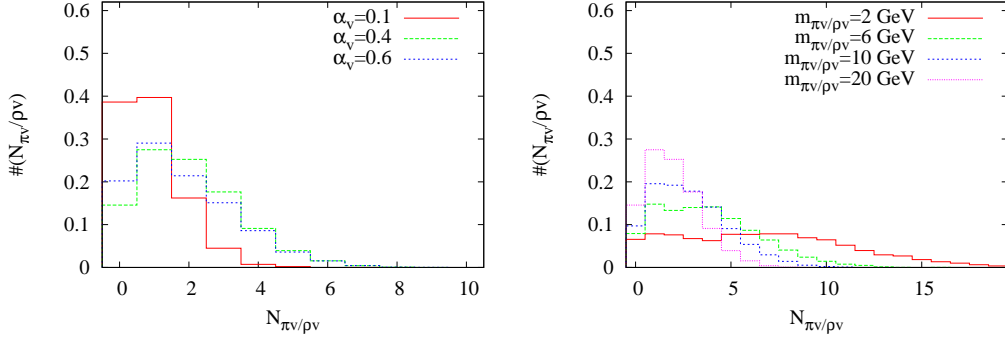


**Figure 13:**  $KMNA_{\gamma_v}$ : the number of flavour diagonal  $\pi_v/\rho_v$  gauge bosons emitted per event. On the left we emphasize the  $\alpha_v$  dependence, while on the right the  $m_{\pi_v/\rho_v}$  dependence. On the left side  $m_{\pi_v/\rho_v} = 10$  GeV and  $\alpha_v = 0.1, 0.4, 0.6$ , while on the right side  $m_{\pi_v/\rho_v} = 2, 6, 10, 20$  GeV and the coupling is fixed at  $\alpha_v = 0.4$ .

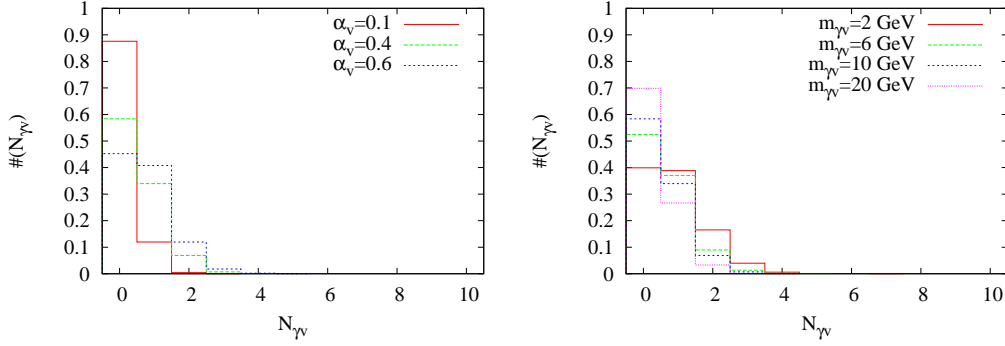


**Figure 14:**  $SMA$ : the number of  $\gamma_v$  gauge bosons emitted per event. On the left we emphasize the  $\alpha_v$  dependence, while on the right the  $m_{\gamma_v}$  dependence. In both plots  $m_{E_v} = 250$  GeV and  $m_{q_v} = 50$  GeV. On the left side  $m_{\gamma_v} = 10$  GeV and  $\alpha_v = 0.1, 0.4, 0.6$ , while on the right side  $m_{\gamma_v} = 2, 6, 10, 20$  GeV and the coupling is fixed at  $\alpha_v = 0.4$ .

while the rest are less so. A reasonable first approximation is to associate the highest energy electron and positron with the two  $E_v$  decays, and the rest with the  $\gamma_v/\pi_v/\rho_v$  ones. The curve in Fig. 16 represents the sum of the steeply falling spectrum associated to the leptons coming from  $\gamma_v$  decay, and a flat spectrum associated to the leptons from  $E_v \rightarrow eq_v$  decay. The upper and lower shoulders of the former energy distributions then give a relationship between the  $E_v$  and the  $q_v$  masses [18].

#### 4.5 Angular distributions and event shapes

The distribution of the production cross-section as a function of the angle between the jets and the beam axis has a characteristic dependence on the spin of the pair-produced particles. This fact may be used to identify the  $q_v$  spin.

In Fig. 17 one may observe the  $\cos \theta_i$  distribution, where  $\theta_i$  is the polar angle between the  $i^{\text{th}}$  jet and the beam axis, for  $m_{\gamma_v} = 10$  GeV. Only jets with a reconstructed mass

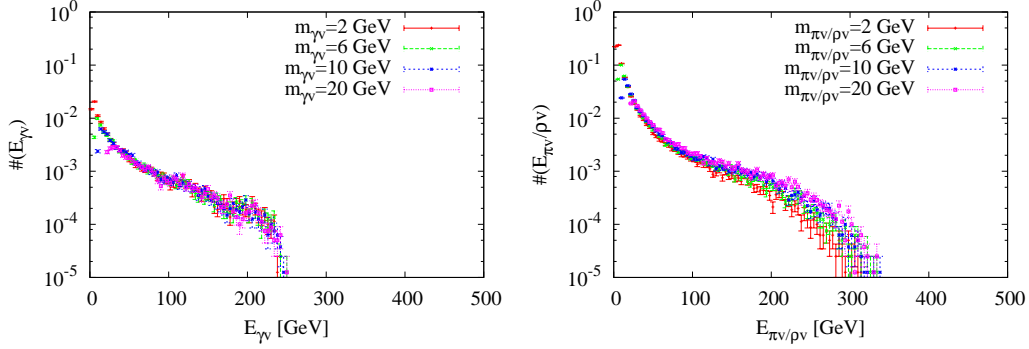


**Figure 15:** *SMA* vs *SMNA*: the energy spectra of the  $\gamma_v$  and of the diagonal  $\pi_v/\rho_v$  emitted per event. The left side shows the energy distribution for *SMA*  $m_{E_v} = 250$ , GeV  $m_{q_v} = 50$  GeV, the right side shows the corresponding distribution for *SMNA* (in this case  $m_{q_v} = 1, 3, 5, 10$  GeV corresponds to half of the  $\pi_v/\rho_v$  mass.).

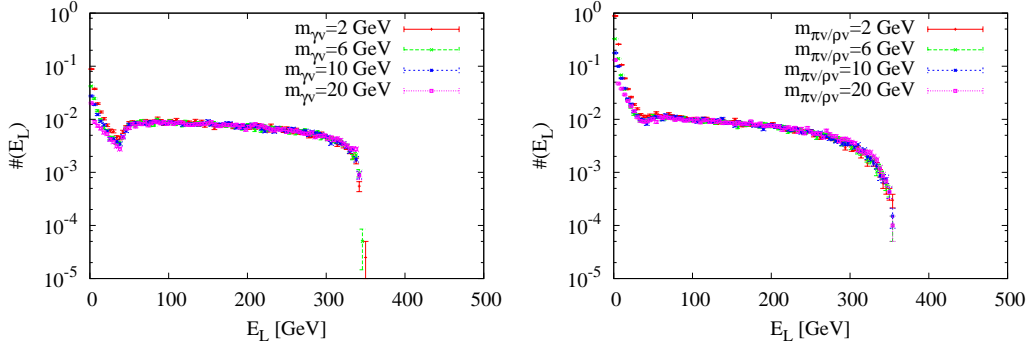


**Figure 16:** *SMA* vs *SMNA*: the lepton energy spectra in the Abelian (left) case and in the non-Abelian (right) case. In the Abelian case GeV  $m_{q_v} = 50$  GeV, while in the non-Abelian case  $m_{q_v} = 1, 3, 5, 10$  GeV. In both cases  $m_{E_v} = 250$  GeV.

$m_j > m_{\gamma_v}/2$  are shown, since lower-mass jets are strongly contaminated by ISR photons above the  $\theta_{\text{cut}} = 50$  mrad cut. The production cross-section for  $e^+e^- \rightarrow q_v\bar{q}_v$ , with  $q_v$  a massless spin 1/2 fermion, is proportional to  $1 + \cos^2 \theta$ . In the  $\text{AM}_{Z'}$  case one must allow for corrections due to the  $\theta_{\text{cut}}$ , to the  $q_v$  being massive and to the  $\gamma_v$  radiation; typically this leads to a somewhat flatter distribution. In the *SMA* case the isotropic decays  $E_v \rightarrow eq_v$  flattens whatever original  $e^+e^- \rightarrow E_v\bar{E}_v$  distribution, unless the  $eq_v$  decay products are highly boosted. In our case a small ISR contamination is still visible close to  $\cos \theta = 1$ , but otherwise the distribution is flat.

The distribution of opening angles in pairs of  $v$ -particles,  $\theta_{ij}$ , should give some insight whether the secluded sector  $G$  is an Abelian or a confining non-Abelian group. In an Abelian event the  $q_v\bar{q}_v$  quarks define a dipole emission axis. To first approximation the  $v$ -gammas are emitted independently, i.e. with a flat distribution in the  $\phi$  angle around the dipole axis, and uniformly in rapidity along this axis. In the non-Abelian case the emissions occur along a chain of dipoles, that is reconfigured by each new emission, since

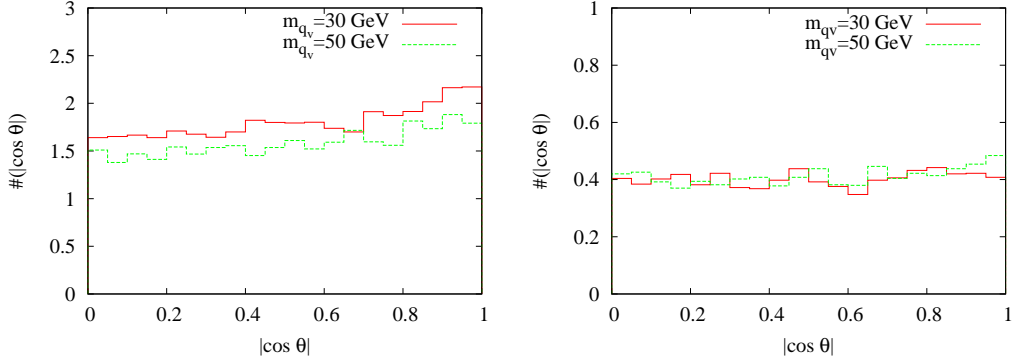


**Figure 17:**  $AM_{Z'}$  and  $SMA$ : the distribution of  $\cos \theta_i$ , where  $\theta_i$  is the angle between the  $i^{\text{th}}$  jet and the beam axis, for  $m_{q_v} = 30$  GeV and for  $m_{q_v} = 50$  GeV. A lower cut on the invariant mass  $m_j > m_{\gamma_v/\pi_v/\rho_v}/2$  was applied in this case. In both cases  $m_{\gamma_v} = 10$  GeV and the  $v$ -coupling is fixed to  $\alpha_v = 0.4$ ,  $m_{q_v} = 10$  GeV.

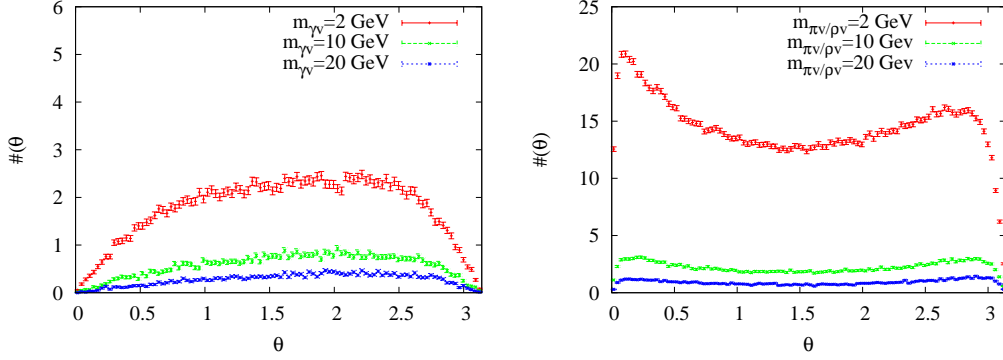


**Figure 18:**  $AM'_Z$  and  $NAM'_Z$ : the distribution of  $\theta_{ij}$ , the angle between the  $\gamma_v$ s in the Abelian case (left), or the angle between the diagonal mesons in the non-Abelian case (right). The distributions are shown as functions of the mass  $m_{\gamma_v} = m_{\pi_v/\rho_v}$ . The coupling constant is  $\alpha_v = 0.4$  in both cases. Note that the number of  $\gamma_v$  and diagonal  $\pi_v/\rho_v$  is different in the two cases.

the  $g_v$ s carry  $v$ -colour charge. This implies a different underlying correlation structure, but it is unclear what happens with this correlation on the way through the  $v$ -hadronization process and the decays back into the standard sector, and how best to search for it.

In Fig. 18 we show the  $\theta_{ij}$  distribution of  $v$ -particle pairs, for the Abelian  $AM_{Z'}$  and non-Abelian  $NAM_{Z'}$  cases. Note how the  $\theta_{ij} 0$  and  $\theta_{ij} \pi$  angles are preferred in non-Abelian case. The comparison is somewhat misleading, however, in the sense that we compare scenarios with the same  $m_{\gamma_v} = m_{\pi_v/\rho_v}$  and the same  $\alpha_v$ , but with different numbers of  $v$ -particles per event (see Fig. 4) and different  $v$ -particle energy distributions. In Sec. 5 we will discuss further these distributions under more similar conditions.

In Fig. 19 we show the reconstructed jet-jet  $\cos \theta_{ij}$  distributions corresponding to the  $v$ -particle distributions in Fig. 18. Note how the relative difference between the Abelian and non-Abelian scenarios is maintained.

In order to characterize the shape of the events one may also use thrust and (the

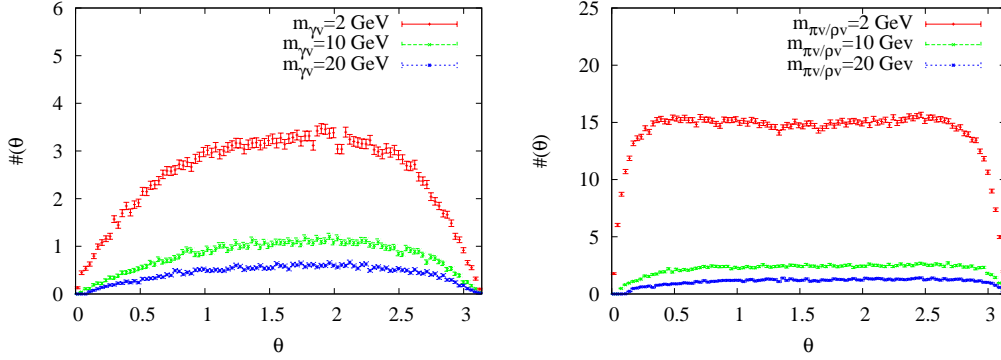


**Figure 19:**  $AM'_Z$  and  $NAM'_Z$ : the distribution of  $\theta_{ij}$ , the angle between the jets in the Abelian case (left) and in the non-Abelian case (right). The distributions are shown as functions of the mass  $m_{\gamma_v} = m_{\pi_v/\rho_v}$ . The  $v$ -coupling is fixed to  $\alpha_v = 0.4$ .

linearized version of) sphericity [39, 40, 41]. These indicate whether an event is more pencil-like,  $T=1$  and  $S=0$ , or more spherical,  $T=1/2$  and  $S=1$ . Sphericity and thrust are primarily intended for events analyzed in their own rest frame, while the visible systems we study have a net momentum that is compensated by the stable secluded-sector particles, plus ISR photons going down the beam pipe and neutrinos. Since we are interested in the properties of the visible system itself, not in its net motion, the analysis is performed in the rest frame of this visible system. In addition, for the SMA scenarios, a further distortion occurs by the kinematics of the  $E_v \rightarrow eq_v$  decays, and by the presence of the resulting  $e^\pm$  in the final state. To this end, the highest-energy electron and positron are excluded from the definition of the visible system.

In Fig. 20 we show the thrust distributions in the six scenarios, and in Fig. 21 the sphericity distributions. As one may have predicted, the events become less pencil-like as the coupling  $\alpha_v$  grows. In addition the SM mediated events are less likely to be pencil-like than the KM or  $Z'$  mediated ones. Note that events with smaller  $\alpha_v$ , in which nothing is radiated are not analyzed.

## 5. Analysis: comparing $\mathcal{U}(1)$ and $SU(N)$

In this section we begin to address the issue of discriminating between Abelian and non-Abelian scenarios in cases in which smoking-gun discriminating signals are absent. To this end we consider the most challenging scenario, in which  $\gamma_v$  and  $\pi_v, \rho_v$  have the same mass, and the same average number of  $v$ -particles leak back into the SM sector, carrying the same average amount of energy. We also consider the same production mechanism, to reduce model dependence and to isolate the effects of the hidden sector dynamics.

So how could the Abelian and non-Abelian scenarios come to have so similar properties? First off, of course,  $m_{\gamma_v} = m_{\pi_v} = m_{\rho_v}$  needs to be assumed. Thereafter the value of  $N_{\text{flav}}$  in the non-Abelian model specifies that exactly an average fraction  $1/N_{\text{flav}}$  of the full energy leaks back into the visible sector. In the Abelian model, for a given  $m_{q_v}$ ,  $\alpha_v$  is the only free parameter that could be fixed to give that average energy. For this parameter



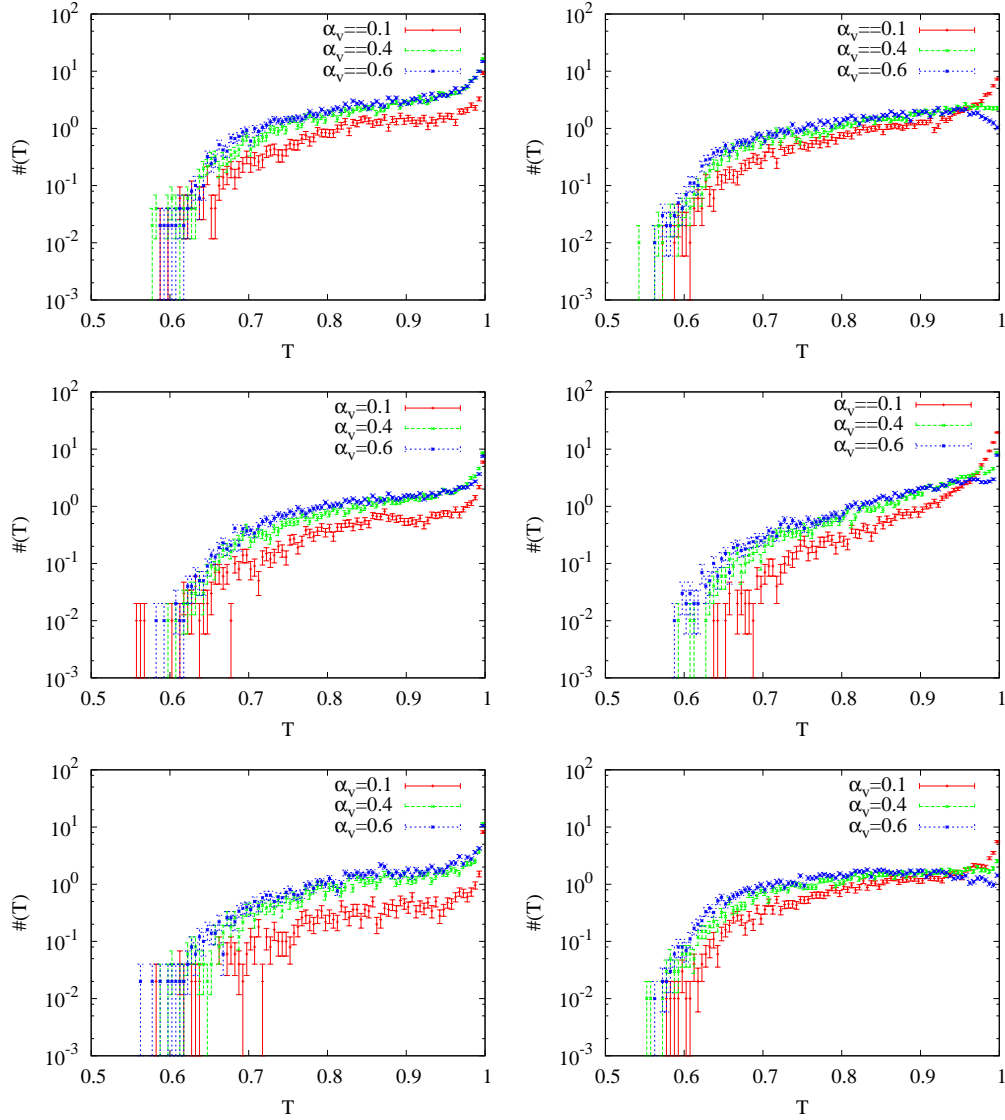


**Figure 20:** The plots show the thrust distribution for the six scenarios as a function of the  $\alpha_v$ . These correspond to, from top to bottom,  $M_{Z'}$ ,  $KM\gamma_v$  and SM production. The plots on the left show the Abelian case while the plot on the right show the non-Abelian cases. For all Abelian plots, the parameters are set to  $m_{q_v} = 50$  GeV and  $m_{\gamma_v} = 10$  GeV. For the SMA case  $m_{E_v} = 250$  GeV is set as well. For the non-Abelian cases, the mass of the mesons is fixed to  $m_{\gamma_v}/\pi_v/\rho_v$

set, the number and energy spectrum of  $\gamma_v$ s are predicted entirely by the perturbative cascade. These distributions now need to be roughly reproduced by the non-Abelian model, which first of all means the same average number of  $v$ -particles decaying back into the SM. While  $m_{q_v} = m_{\pi_v}/2$  is fixed in this case, there is freedom in the choices of  $\alpha_v$  and non-perturbative fragmentation parameters. Recall that the number of  $v$ -particles will not vanish in the  $\alpha_v \rightarrow 0$  limit for the non-Abelian model, unlike the Abelian one. Actually it turns out to be slightly difficult to reduce the non-Abelian multiplicity down to the level set by the Abelian scenario. With an  $\alpha_v$  comparable to that of a QCD cascade at a cor-

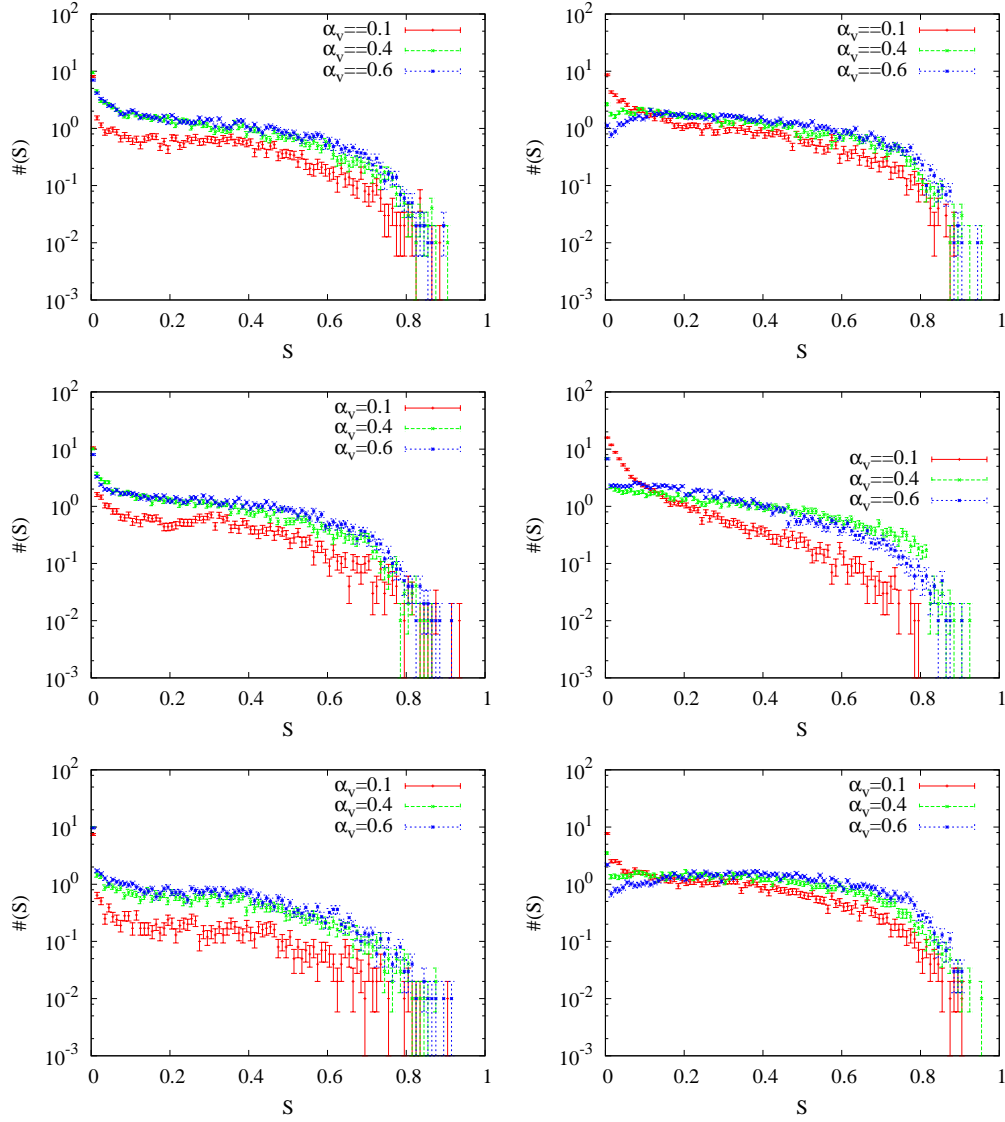


**Figure 21:** The plots show the (linearized) sphericity distribution for the six scenarios as a function of the  $\alpha_v$ . These correspond to, from top to bottom,  $\text{KM}_{Z'}$ ,  $\text{KM}_{\gamma_v}$  and SM production. The plots on the left show the Abelian case while the plot on the right show the non-Abelian cases. For all Abelian plots, the parameters are set to  $m_{q_v} = 50$  GeV and  $m_{\gamma_v} = 10$  GeV. For the SMA case  $m_{E_v} = 250$  GeV is set as well. For the non-Abelian cases, the mass of the mesons is fixed to  $m_{\pi_v/\rho_v} = m_{\gamma_v}$ .

responding energy/mass ratio, the longitudinal fragmentation function needs to be made harder by decreasing  $a$  and increasing  $b'$  relative to the QCD values.

Using such a strategy, a matching pair of scenarios have been constructed, an  $\text{AM}'_Z$  model with  $m_{q_v} = 20$  GeV,  $m_{\gamma_v} = 10$  GeV and  $\alpha_v = 0.3$ , and a  $\text{NAM}'_Z$  with  $m_{q_v} = 5$  GeV,  $m_{\pi_v/\rho_v} = 10$  GeV,  $N_{\text{flav}} = 4$ ,  $\alpha_v = 0.15$ ,  $a = 0.12$  and  $b' = 2$ . This gives fair agreement, as can be seen in Fig. 22.

We can now compare the angular distributions in the two cases. In Fig. 23 (left) one

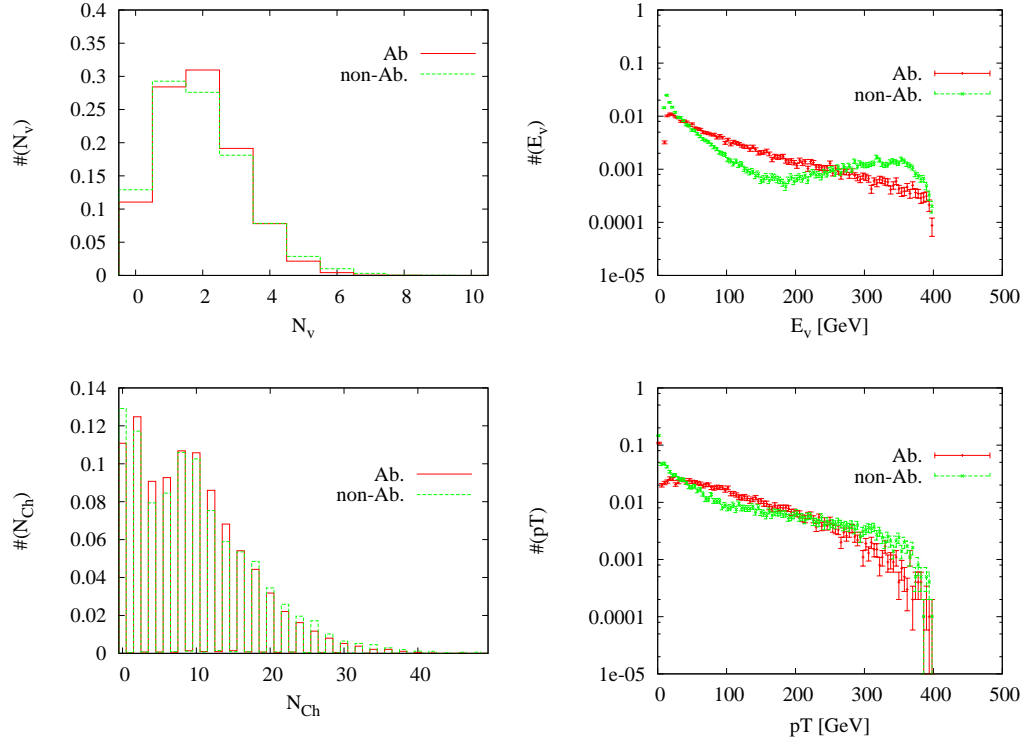


**Figure 22:** The plots show the comparison between the Abelian and the non-Abelian setups: the number of  $\gamma$ s (Abelian) or diagonal  $\pi$ s/ $\rho$ s (non-Abelian) (top left), the  $v$ -particle energy distribution (top right), the number of SM charged particles produced, and the missing  $p_{\perp}$ . The scenarios are chosen to yield similar distributions.

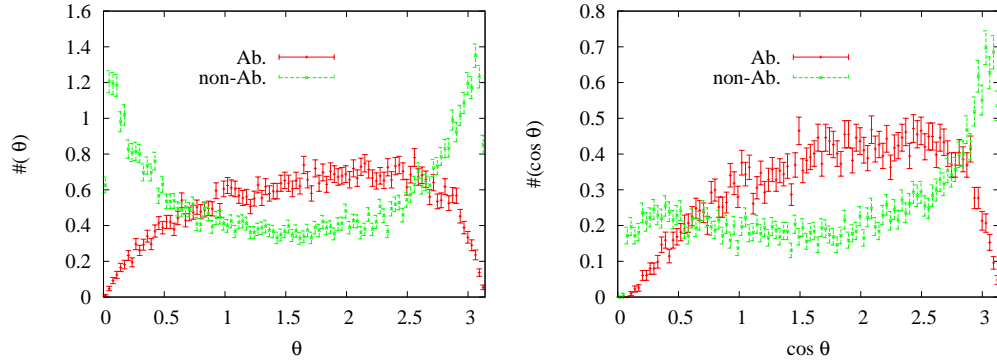


**Figure 23:** The plots show the comparison between the Abelian and the non Abelian setups. On the left is the  $\cos \theta_{ij}$  between the  $v$ -particles which can decay back into the SM. On the right is the corresponding  $\cos \theta_{ij}$  between the jets in the detector.

may observe how in the non-Abelian case the  $\theta_{ij}$  distribution of the angle between the visible  $v$ -particles is much more peaked near 0 and  $\pi$  than in the Abelian one. The plot on the right shows how this characteristic is maintained in jet distributions.

We have repeated the study for some different model parameters and found similar

results. In the second comparison the  $AM'_Z$  model has  $m_{q_v} = 50$  GeV,  $m_{\gamma_v} = 10$  GeV and  $\alpha_v = 0.43$ , while  $NAM'_Z$  has  $m_{q_v} = 5$  GeV,  $m_{\pi_v/\rho_v} = 10$  GeV,  $N_{\text{flav}} = 4$ ,  $\alpha_v = 0.18$ ,  $a = 0.2$  and  $b' = 2$ .

It is tempting to ascribe the observed differences to different radiation/hadronization patterns in the two scenarios, ultimately deriving from the different dipole emission topologies already discussed. One attractive possibility is that the relative lack of peaking at  $\cos\theta_{ij} = \pm 1$  for the Abelian scenario is a consequence of the dead cone effect, i.e. the suppression of emissions parallel to a massive radiating particle. A back-to-back  $q_v\bar{q}_v$  pair undergoing non-Abelian hadronization would have no corresponding suppression for  $v$ -hadron formation along this axis. However, considering of the flexibility that exists in the tuning of non-perturbative hadronization parameters, and the differences observed in the  $v$ -particle energy spectrum, we will not now be as bold as to exclude the possibility of a closer match. If such a match required straining the non-perturbative model to behave rather differently from QCD extrapolations, however, then such tunes would not be particularly credible.

## 6. Summary and Outlook

In this article we have compared six different scenarios of a generic secluded-sector character. These are either kinetic mixing with a light  $\gamma_v$ , or  $Z'$ , or new  $F_v$  particles, and in each case either with a broken  $U(1)$  or an unbroken  $SU(N)$ . The  $F_v$  particles are charged both under the Standard Model groups and the new secluded-sector groups, and so are guaranteed a significant production rate, whenever kinematically possible, whereas the rate via  $\gamma_v$  or  $Z'$  depends on a number of parameters such as the  $\gamma/\gamma_v$  mixing parameters or the  $Z'$  coupling structure and mass. In this article we have completely disregarded such rate issues and instead studied the properties of the different models on an event-by-event basis.

In order to do so, we have developed a new flexible framework that implements hadronization in the hidden sector. Similar modeling in the past have relied on simple rescaling of QCD, whereas here we set up hidden-sector string fragmentation as a completely separate framework, though sharing the same underlying space-time structure of the hadronization process. We have also expanded on our previous work with parton showers in the hidden sector, possibly interleaved with radiation in the visible sector, by allowing for the emission of massive  $\gamma_v$ s, when the  $U(1)$  group is broken. In order to obtain the correct behaviour, both in the soft/collinear limits and for hard emissions, the shower is matched to first-order matrix elements we have calculated for the massive  $\gamma_v$  cases. Much of the framework presented here could be applied also to other related scenarios, although there are limits. For instance, implicitly it has been assumed that the  $q_v$  masses are not too dissimilar from the confinement scale  $\Lambda$  of the new  $SU(N)$  group — hadronization would look rather different in the limit  $m_{q_v} \gg \Lambda$ .

In the scenarios where  $F_v$ s are produced and promptly decay like  $F_v \rightarrow fq_v$ , the presence of the fermions  $f$  in the final state is a distinguishing factor, and the  $f$  energy spectrum can be used to extract information on mass scales in the secluded sector. At

first glance, the production mediated by a  $\gamma_v$  or a  $Z'$  would seem to be more similar. The different location of the propagator mass peaks leads to quite significant patterns of initial-state photon radiation, however, that would be easily observed.

The challenge, thus, is to distinguish an Abelian and a non-Abelian scenario interactions in the secluded sector. In certain cases that would be straightforward, e.g. if there is only one  $q_v$  species, so that all energy decays back into the standard sector in the non-Abelian models. It is possible to fix parameters in the non-Abelian cases so that only some fraction decays, so that the level of activity matches Abelian  $\alpha_v$  one.

Our first investigations here point to differences showing up in event properties related to the overall structure of the energy and particle flow. More elaborate tunings possibly might bring the models closer together, but one would hope that data still would favour “what comes naturally” in either of the models.

There are also more handles than the ones we have used. We have shown that not only lepton pairs but also jets are amenable to mass peak identification, which would allow to divide events into several subsystems and analyze their relative location, e.g. searching for coherence effects. Should lifetimes be long enough to induce displaced vertices, not only would that be a spectacular signal, but it would also be a boon to such analysis efforts.

The most obvious next step would be to study these models for consequences at the LHC. The task can be split into three parts: cross sections, triggers and model-specific event properties. The cross sections are so intimately related to the choice of masses and couplings that it will be impossible to exclude the possibility of a secluded sector, only to separate excluded and not-excluded regions of parameter space, in close analogy with SUSY. The obvious trigger would be  $\cancel{p}_\perp$ , but we have seen that this would not work for non-Abelian scenarios with one  $q_v$  flavour. It would then need to be supplemented by the presence of (multiple) lepton pairs of some fixed invariant mass and, if we are lucky, displaced vertices. The final step would be to understand whether the more busy environment in hadronic events would still allow to distinguish Abelian and non-Abelian models — the separation between the three production scenarios we have considered here should still be straightforward. Chances are that this will bring us full circle to the cross sections issue, since more sophisticated analyses will require a decent event rate to start out from.

## Acknowledgments

We would like to thank Matt Strassler, Katryn Zurek, Peter Skands and Bob McElrath for helpful suggestions. Work supported in part by Marie-Curie Early Stage Training program “HEP-EST” (contract number MEST-CT-2005-019626), by the Marie-Curie MC-net program, and by the Swedish Research Council (contract numbers 621-2010-3326 and 621-2008-4219)

## A. Scenario selection and setup

We here present some information relevant to get going with secluded-sector event gener-

name	name	identity	comment
$D_v$	Dv	4900001	partner to the $d$ quark
$U_v$	Uv	4900002	partner to the $u$ quark
$S_v$	Sv	4900003	partner to the $s$ quark
$C_v$	Cv	4900004	partner to the $c$ quark
$B_v$	Bv	4900005	partner to the $b$ quark
$T_v$	Tv	4900006	partner to the $t$ quark
$E_v$	Ev	4900011	partner to the $e$ lepton
$\nu_{E_v}$	nuEv	4900012	partner to the $\nu_e$ neutrino
$M_v$	MUv	4900013	partner to the $\mu$ lepton
$\nu_{M_v}$	nuMUv	4900014	partner to the $\nu_\mu$ neutrino
$T_v$	TAUv	4900015	partner to the $\tau$ lepton
$\nu_{T_v}$	nuTAUv	4900016	partner to the $\nu_\tau$ neutrino
$g_v$	gv	4900021	the $v$ -gluon in an $SU(N)$ scenario
$\gamma_v$	gammav	4900022	the $v$ -photon in a $U(1)$ scenario
$Z', Z_v$	Zv	4900023	massive gauge boson linking SM- and $v$ -sectors
$q_v$	qv	4900101	matter particles purely in $v$ -sector
$\pi_v^{\text{diag}}$	pivDiag	4900111	flavour-diagonal spin 0 $v$ -meson
$\rho_v^{\text{diag}}$	rhovDiag	4900113	flavour-diagonal spin 1 $v$ -meson
$\pi_v^{\text{up}}$	pivUp	4900211	flavour-nondiagonal spin 0 $v$ -meson
$\rho_v^{\text{up}}$	rhovUp	4900213	flavour-nondiagonal spin 1 $v$ -meson
	ggv	4900991	glueball made of $v$ -gluons

**Table 2:** The allowed new particles in valley scenarios. Names are gives as used in this text and as in PYTHIA 8 event listings. The identity code is an integer identifier, in the spirit of the PDG codes, but is not part of the current PDG standard [38].

ation in PYTHIA 8. Basic knowledge of the program is assumed [25].

The  $v$ -particle content is summarized in Tab. 2. Needless to say, not all of them would be relevant for each specific scenario. Internally further copies of  $q_v$  may be used, up to code 4900108, but these do not appear in the event record. Properties of the particles can be set to modify the scenarios, notably mass (`m0`); only the  $g_v$  must remain massless. If  $F_v \rightarrow f q_v$  is allowed, masses must be chosen so that the decay is kinematically possible. The  $\pi_v$  and  $\rho_v$  masses should be set at around twice the  $q_v$  one. For unstable particles the width (`mWidth`) and allowed mass range (`mMin` and `mMax`) can be set. To generate displaced vertices the  $c\tau$  value must be set (`tau0`). Spin choices are described later.

Several particles by default are set stable, so it is necessary to switch on their decay (`mayDecay`). For  $\gamma_v$ ,  $\pi_v^{\text{diag}}$  and  $\rho_v^{\text{diag}}$  no decay channels are on by default, since that set depends so strongly on the mass scale selected. The simple way, of switching on everything (`onMode = on`) works in principle, but e.g. a 10 GeV  $\gamma_v$  would then be above the  $b\bar{b}$  threshold but below the  $B\bar{B}$  one, and so generate a trail of (harmless) error messages. Also the branching ratios of the decay channels may need to be adjusted, based on the scenario. The  $Z_v$  ones are mainly place-fillers, to give one example.

code	flag	process
4901	HiddenValley:gg2DvDvbar	$gg \rightarrow D_v \bar{D}_v$
4902	HiddenValley:gg2UvUvbar	$gg \rightarrow U_v \bar{U}_v$
4903	HiddenValley:gg2SvSvbar	$gg \rightarrow S_v \bar{S}_v$
4904	HiddenValley:gg2CvCvbar	$gg \rightarrow C_v \bar{C}_v$
4905	HiddenValley:gg2BvBvbar	$gg \rightarrow B_v \bar{B}_v$
4906	HiddenValley:gg2TvTvbar	$gg \rightarrow T_v \bar{T}_v$
4911	HiddenValley:qqbar2DvDvbar	$q\bar{q} \rightarrow g^* \rightarrow D_v \bar{D}_v$
4912	HiddenValley:qqbar2UvUvbar	$q\bar{q} \rightarrow g^* \rightarrow U_v \bar{U}_v$
4913	HiddenValley:qqbar2SvSvbar	$q\bar{q} \rightarrow g^* \rightarrow S_v \bar{S}_v$
4914	HiddenValley:qqbar2CvCvbar	$q\bar{q} \rightarrow g^* \rightarrow C_v \bar{C}_v$
4915	HiddenValley:qqbar2BvBvbar	$q\bar{q} \rightarrow g^* \rightarrow B_v \bar{B}_v$
4916	HiddenValley:qqbar2TvTvbar	$q\bar{q} \rightarrow g^* \rightarrow T_v \bar{T}_v$
4921	HiddenValley:ffbar2DvDvbar	$f\bar{f} \rightarrow \gamma^* \rightarrow D_v \bar{D}_v$
4922	HiddenValley:ffbar2UvUvbar	$f\bar{f} \rightarrow \gamma^* \rightarrow U_v \bar{U}_v$
4923	HiddenValley:ffbar2SvSvbar	$f\bar{f} \rightarrow \gamma^* \rightarrow S_v \bar{S}_v$
4924	HiddenValley:ffbar2CvCvbar	$f\bar{f} \rightarrow \gamma^* \rightarrow C_v \bar{C}_v$
4925	HiddenValley:ffbar2BvBvbar	$f\bar{f} \rightarrow \gamma^* \rightarrow B_v \bar{B}_v$
4926	HiddenValley:ffbar2TvTvbar	$f\bar{f} \rightarrow \gamma^* \rightarrow T_v \bar{T}_v$
4931	HiddenValley:ffbar2EvEvbar	$f\bar{f} \rightarrow \gamma^* \rightarrow E_v \bar{E}_v$
4932	HiddenValley:ffbar2nuEvnuEvbar	$f\bar{f} \rightarrow \gamma^* \rightarrow \nu_{E_v} \bar{\nu}_{E_v}$
4933	HiddenValley:ffbar2MUvMUvbar	$f\bar{f} \rightarrow \gamma^* \rightarrow M_v \bar{M}_v$
4934	HiddenValley:ffbar2nuMUvnuMUvbar	$f\bar{f} \rightarrow \gamma^* \rightarrow \nu_{M_v} \bar{\nu}_{M_v}$
4935	HiddenValley:ffbar2TAUvTAUvbar	$f\bar{f} \rightarrow \gamma^* \rightarrow T_v \bar{T}_v$
4936	HiddenValley:ffbar2nuTAUvnuTAUvbar	$f\bar{f} \rightarrow \gamma^* \rightarrow \nu_{T_v} \bar{\nu}_{T_v}$
4941	HiddenValley:ffbar2Zv	$f\bar{f} \rightarrow Z_v^* (\rightarrow q_v \bar{q}_v)$

**Table 3:** Allowed processes that can be switched on individually.

The list of processes is shown in Tab. 3. It would be possible to switch on all of them with `HiddenValley:all = on`, but normally that would imply a mix of different scenarios that does not appear plausible. Many processes should also be viewed in the context of the other choices made.

Finally, the list of relevant model parameters is shown in Tab. 4. On top is the choice between a  $U(1)$  and an  $SU(N)$  scenario. The  $F_v$  and  $q_v$  spins must be selected in a coordinated fashion, to be consistent with  $F_v \rightarrow f q_v$  decays. The choice of  $F_v$  spin directly affects the process (differential) cross sections. If  $F_v$  has spin 1 also the choice of an anomalous magnetic moment would have an influence.

The kinetic mixing switch allows to reuse the  $\gamma^*$ -mediated processes in a completely different context than originally foreseen, in which the  $F_v$  have no Standard Model coupling but are produced by  $\gamma - \gamma_v$  mixing. Actually this redefines the  $F_v$  to be equivalent with what we normally call  $q_v$ . Thus a process like  $f\bar{f} \rightarrow \gamma^* \rightarrow E_v \bar{E}_v$  becomes  $f\bar{f} \rightarrow \gamma^* \rightarrow \gamma_v^* \rightarrow q_v \bar{q}_v$ . To complete this transformation you need to set the  $E_v$  stable (`mayDecay =`

parameter	def.	meaning
Scenario		
HiddenValley:Ngaug	3	1 for $U(1)$ , $N$ for $SU(N)$
HiddenValley:spinFv	1	0, 1 or 2 for $F_v$ spin 0, 1/2 and 1
HiddenValley:spinqv	0	$q_v$ spin 0 or 1 when $s_{F_v} = 1/2$
HiddenValley:kappa	1.	$F_v$ anomalous magnetic dipole moment
HiddenValley:doKinMix	off	allow kinetic mixing
HiddenValley:kinMix	1.	strength of kinetic mixing, if on
Showers in secluded sector		
HiddenValley:FSR	off	allow final-state radiation
HiddenValley:alphaFSR	0.1	constant coupling strength
HiddenValley:pTminFSR	0.4	lower cutoff of shower evolution
Hadronization in secluded sector		
HiddenValley:fragment	off	allow hadronization
HiddenValley:nFlav	1	$N_{\text{flav}}$ , number of distinct $q_v$ species
HiddenValley:probVector	0.75	fraction of spin-1 $v$ -mesons
HiddenValley:aLund	0.3	$a$ parameter in eq. (A.1)
HiddenValley:bmqv2	0.8	$b' = bm_{q_v}^2$ parameter in eq. (A.1)
HiddenValley:rFactqv	1.0	$r$ parameter in eq. (A.1)
HiddenValley:sigmamqv	0.5	$\sigma'$ , such that $\sigma = \sigma' m_{q_v}$

**Table 4:** The parameters that can be set to select the model to study, with default values and some explanations.

false), uncharged (`chargeType` = 0) and invisible (`isVisible` = false).

The shower parameters should be self-explanatory. The lower cutoff scale can be raised in proportion to the characteristic mass scales, but ought to be no more than  $m_{q_v}/2$ , say. A lower cutoff means longer execution time without any significant change of event properties.

The hadronization parameters have also been discussed before, except for  $r$ , which is providing slightly more flexibility to the Lund–Bowler fragmentation function than in eq. (3.26)

$$f(z) \propto \frac{1}{z^{1+rb'}} (1-z)^a \exp\left(-\frac{b'm_{m_v}^2}{z m_{m_q}^2}\right). \quad (\text{A.1})$$

where  $r$  could be set anywhere between 0 and 1. The dimensionless  $\sigma'$  parameter is normalized so that the  $q_v$  of each new pair produced in the hadronization has a  $\langle p_\perp^2 \rangle = (\sigma' m_{q_v})^2$ .

Behind the scenes, the `HiddenValleyFragmentation` class can reuse most of the standard `StringFragmentation` and `MiniStringFragmentation` machineries. Specifically, already for the Standard Model hadronization, the selection of flavour,  $z$  and  $p_\perp$  is relegated to three “helper” classes. The three new classes `HVStringFlav`, `HVStringZ` and `HVStringPT` derive from their respective SM equivalent, and cleanly replace these three aspects while keeping the rest of the handling of complex string topologies. Specifically, it would be straightforward to expand towards a richer flavour structure in the secluded sector. Note, however, that it is important to select  $v$ -quark “constituent” masses that reasonably match



the intended  $v$ -meson mass spectrum, since such relations are assumed in parts of the code. Furthermore, with new  $q_v$  defined with separate particle data, one must disable the few lines in `HiddenValleyFragmentation::init(...)` that now duplicate the one  $q_v$  into several identical copies.

## References

- [1] M. J. Strassler and K. M. Zurek, “Echoes of a hidden valley at hadron colliders,” *Phys. Lett. B* **651**, 374 (2007) [arXiv:hep-ph/0604261].
- [2] M. J. Strassler, K. M. Zurek, “Discovering the Higgs through highly-displaced vertices,” *Phys. Lett. B* **661** (2008) 263-267. [hep-ph/0605193].
- [3] M. J. Strassler, “Possible effects of a hidden valley on supersymmetric phenomenology,” arXiv:hep-ph/0607160.
- [4] T. Han, Z. Si, K. M. Zurek *et al.*, “Phenomenology of hidden valleys at hadron colliders,” *JHEP* **0807** (2008) 008. [arXiv:0712.2041 [hep-ph]].
- [5] M. J. Strassler, “Why Unparticle Models with Mass Gaps are Examples of Hidden Valleys,” arXiv:0801.0629 [hep-ph].
- [6] M. J. Strassler, “On the Phenomenology of Hidden Valleys with Heavy Flavor,” arXiv:0806.2385 [hep-ph].
- [7] J. E. Juknevich, D. Melnikov, M. J. Strassler, “A Pure-Glue Hidden Valley I. States and Decays,” *JHEP* **0907** (2009) 055. [arXiv:0903.0883 [hep-ph]].
- [8] N. Arkani-Hamed, D. P. Finkbeiner, T. R. Slatyer *et al.*, “A Theory of Dark Matter,” *Phys. Rev. D* **79** (2009) 015014. [arXiv:0810.0713 [hep-ph]].
- [9] K. M. Zurek, “Multi-Component Dark Matter,” *Phys. Rev. D* **79** (2009) 115002 [arXiv:0811.4429 [hep-ph]].
- [10] M. Baumgart, C. Cheung, J. T. Ruderman *et al.*, “Non-Abelian Dark Sectors and Their Collider Signatures,” *JHEP* **0904** (2009) 014. [arXiv:0901.0283 [hep-ph]].
- [11] C. Cheung, J. T. Ruderman, L. -T. Wang *et al.*, “Kinetic Mixing as the Origin of Light Dark Scales,” *Phys. Rev. D* **80** (2009) 035008. [arXiv:0902.3246 [hep-ph]].
- [12] D. E. Morrissey, D. Poland, K. M. Zurek, “Abelian Hidden Sectors at a GeV,” *JHEP* **0907** (2009) 050. [arXiv:0904.2567 [hep-ph]].
- [13] O. Adriani *et al.*, “A new measurement of the antiproton-to-proton flux ratio up to 100 GeV in Phys. Rev. Lett. **102**, 051101 (2009) [arXiv:0810.4994 [astro-ph]].
- [14] O. Adriani *et al.* [ PAMELA Collaboration ], “An anomalous positron abundance in cosmic rays with energies 1.5-100 GeV,” *Nature* **458** (2009) 607-609. [arXiv:0810.4995 [astro-ph]].
- [15] J. Chang, J. H. Adams, H. S. Ahn *et al.*, “An excess of cosmic ray electrons at energies of 300-800 GeV,” *Nature* **456** (2008) 362-365.
- [16] A. A. Abdo *et al.* [ The Fermi LAT Collaboration ], “Measurement of the Cosmic Ray  $e^+$  plus  $e^-$  spectrum from 20 GeV to 1 TeV with the Fermi Large Area Telescope,” *Phys. Rev. Lett.* **102** (2009) 181101. [arXiv:0905.0025 [astro-ph.HE]].
- [17] B. Holdom, “Two U(1)’s and Epsilon Charge Shifts,” *Phys. Lett. B* **166** (1986) 196.

- [18] L. Carloni and T. Sjostrand, “Visible Effects of Invisible Hidden Valley Radiation,” JHEP **1009** (2010) 105 [arXiv:1006.2911 [hep-ph]].
- [19] L. Bergstrom, J. Edsjo, G. Zaharijas, “Dark matter interpretation of recent electron and positron data,” Phys. Rev. Lett. **103** (2009) 031103. [arXiv:0905.0333 [astro-ph.HE]].
- [20] B. McElrath, “Invisible quarkonium decays as a sensitive probe of dark matter,” Phys. Rev. **D72** (2005) 103508. [hep-ph/0506151].
- [21] B. Batell, M. Pospelov, A. Ritz, “Probing a Secluded U(1) at B-factories,” Phys. Rev. **D79** (2009) 115008. [arXiv:0903.0363 [hep-ph]].
- [22] R. Essig, P. Schuster, N. Toro, “Probing Dark Forces and Light Hidden Sectors at Low-Energy e+e- Colliders,” Phys. Rev. **D80** (2009) 015003. [arXiv:0903.3941 [hep-ph]].
- [23] M. Reece, L. -T. Wang, “Searching for the light dark gauge boson in GeV-scale experiments,” JHEP **0907** (2009) 051. [arXiv:0904.1743 [hep-ph]].
- [24] J. Kang and M. A. Luty, “Macroscopic Strings and ‘Quirks’ at Colliders,” JHEP **0911**, 065 (2009) [arXiv:0805.4642 [hep-ph]].
- [25] T. Sjöstrand, S. Mrenna and P. Z. Skands, “A Brief Introduction to PYTHIA 8.1,” Comput. Phys. Commun. **178**, 852 (2008) [arXiv:0710.3820 [hep-ph]].
- [26] A. Buckley *et al.*, “General-purpose event generators for LHC physics,” arXiv:1101.2599 [hep-ph].
- [27] T. Sjöstrand and P. Z. Skands, Eur. Phys. J. C **39** (2005) 129 [arXiv:hep-ph/0408302].
- [28] E. Norrbin and T. Sjöstrand, “QCD radiation off heavy particles,” Nucl. Phys. B **603**, 297 (2001) [arXiv:hep-ph/0010012].
- [29] R. Corke and T. Sjostrand, “Interleaved Parton Showers and Tuning Prospects,” arXiv:1011.1759 [hep-ph].
- [30] M. Bengtsson and T. Sjostrand, Phys. Lett. B **185** (1987) 435.
- [31] S. Frixione, P. Nason and C. Oleari, JHEP **0711** (2007) 070 [arXiv:0709.2092 [hep-ph]].
- [32] B. Andersson, G. Gustafson, G. Ingelman and T. Sjostrand, Phys. Rept. **97** (1983) 31.
- [33] M. G. Bowler, “e+ e- Production of Heavy Quarks in the String Model,” Z. Phys. **C11** (1981) 169.
- [34] G. ’t Hooft, “A Planar Diagram Theory for Strong Interactions,” Nucl. Phys. **B72** (1974) 461.
- [35] T. Sjostrand, “Jet Fragmentation Of Nearby Partons,” Nucl. Phys. **B248** (1984) 469.
- [36] W. Bartel *et al.* [JADE Collaboration], Phys. Lett. B **160** (1985) 337.
- [37] W. Bartel *et al.* [JADE Collaboration], Z. Phys. C **33** (1986) 23.
- [38] K. Nakamura *et al.* [Particle Data Group], “Review of particle physics,” J. Phys. G **37** (2010) 075021.
- [39] R. K. Ellis, W. J. Stirling and B. R. Webber, Camb. Monogr. Part. Phys. Nucl. Phys. Cosmol. **8**, 1 (1996).
- [40] S. Brandt, C. Peyrou, R. Sosnowski and A. Wroblewski, Phys. Lett. **12**, 57 (1964).
- [41] J. D. Bjorken and S. J. Brodsky, Phys. Rev. D **1**, 1416 (1970).